THESIS FOR THE DEGREE OF DOCTOR OF PHILOSOPHY

Numerical frameworks for simulations of wave energy converter systems: power performance and mooring fatigue analysis in wave energy parks

Xinyuan Shao

Department of Mechanics and Maritime Sciences
CHALMERS UNIVERSITY OF TECHNOLOGY
Gothenburg, Sweden, 2025

Numerical frameworks for simulations of wave energy converter systems: power performance and mooring fatigue analysis in wave energy parks

Xinyuan Shao

ISBN: 978-91-8103-240-6
Doktorsavhandlingar vid Chalmers tekniska högskola
Series number: 5698
ISSN 0346-718X

Chalmers University of Technology
Department of Mechanics and Maritime Sciences
Division of Marine Technology
SE-412 96, Gothenburg
Sweden
Phone: +46 (0)31 772 1000
www.chalmers.se

Typeset by the author using LaTeX.
Printed by Chalmers Reproservice
Gothenburg, Sweden, 2025

Abstract

Wave energy has attracted public attention as an important renewable energy source for many years. Wave energy has many advantages over wind and solar energy, such as around-the-clock availability and high power density. However, further development is needed for wave energy converter (WEC) technology to reach full commercial readiness; in particular, there is an urgent need for a systematic numerical analysis of certain WEC concepts and wave farms to guide their development and design and unleash their enormous potential.

This thesis focuses on the simulation of three point-absorber WEC concepts with different working principles and the wave parks they compose. The primary aim was to develop accurate numerical models and generalised numerical frameworks for the respective WECs and wave parks and analyse their power performance and mooring fatigue damage, two key factors that need to be assessed before wave parks can be commercialised on a large scale.

This thesis contributes to WEC numerical modelling by proposing two numerical frameworks, the DNV SESAM framework and the FMI-based (Functional Mock-up Interface-based) co-simulation framework. The numerical framework refers to the computational structure for modelling WEC systems, in which several numerical methods are integrated to simulate coupled subsystems. The DNV SESAM framework can model WEC systems with some inevitable simplifications in the subsystem models in an integrated software environment. The FMI-based co-simulation framework facilitates convenient coupling between separated solvers and tools without programming and shows great potential for fast inter-team model integration in real industrial applications.

The subsystems of WECs, such as mechanical joint connections and power take-off (PTO) systems, were modelled in detail, thanks to the flexible coupling feature of the proposed FMI-based co-simulation framework. It was found that the fidelity of the subsystem models directly impacts the accuracy of the power performance and mooring fatigue damage predictions, particularly under environmental conditions (ECs) where simplified models cannot capture the nonlinearity introduced by the subsystem. This highlights the necessity of modelling the exact working principles of all subsystems to ensure accurate numerical results.

Various wave parks were modelled and simulated under different ECs. Their power performance and mooring fatigue damage were compared and analysed in detail. The results demonstrate the scope and capabilities of the proposed numerical frameworks, providing valuable insights for modelling and simulating wave parks with different WEC prototypes.

Keywords: DNV SESAM, FMI-based co-simulation, interaction effects, mooring fatigue damage, power performance, wave energy converter (WEC), wave park.

To all who helped and guided me

Acknowledgements

This thesis presents my research from 2021 to 2025 at Chalmers University of Technology. These four challenging and rewarding years have passed by faster than I could have anticipated.

My research was conducted as part of three projects: “Control of wave energy converters based on wave measurements, for optimal energy absorption (WAVEMEASURE)” from 2020 to 2024; “INTERACT - Analysis of array systems of wave energy converters with regard to interaction effects in the LCoE and fatigue analyses” from 2020 to 2024; and “Enhancing Shared mOoring systeM design for flOating Offshore wind faRms (ESOMOOR)” from 2024 to 2025. I sincerely acknowledge the support and collaboration of all my partners in these projects, whose help has been invaluable to this research.

I want to thank my supervisor, Professor Jonas Ringsberg, for all your encouragement and trust. Words cannot fully express my gratitude. You have been not only my supervisor but also my colleague and my friend. I have learned so much from you, especially your dedication to your work and your endless passion for research. It is my greatest honour to have been your student for the past years. You are my role model.

I am grateful to my co-supervisors, Adjunct Professor Erland Johnson, Associate Professor Zhiyuan Li, and Professor Hua-Dong Yao. I immensely enjoyed our discussions and appreciate your assistance in revising my papers and offering valuable suggestions. Special thanks to Professor Hua-Dong Yao. From my Master’s to now, your help and support mean a lot to me.

I would like to thank Professor Peter Folkow for giving me the opportunity to work as a project assistant in 2019. It was then that I had my first taste of doing research. It made me realise that I was interested in doing research, and it pushed me to apply for a PhD later on. That small momentum changes everything.

My journey in research has been full of twists and turns, but every experience, whether good or bad, has shaped me and deepened my reflection on what truly gives life meaning. They make me stronger and more resilient. Therefore, I would also like to express my gratitude for the people and events I encountered in Beijing during 2018–2019.

My friends are a great source of comfort, offering warm hugs and words of support whenever I feel upset. You are indeed a treasure in my life. Our friendship is pure and lasting. I thank Hezhe and her husband, Daoru, Yao, and her cat, Lyapunov, for their unwavering support.

I have enjoyed the work environment in the Division of Marine Technology. I want to thank all my colleagues for creating a welcoming atmosphere in our division. I also want to thank Chalmers for giving me support and equal opportunities to thrive.

Special thanks to my parents and siblings. Though the distance between China

and Sweden physically separates us, it strengthens our bond. Now it is time to share the joy of my graduation with you.

Over the past four years, I have not only gained academic knowledge but also learned how to manage my thoughts and find inner peace. I am deeply grateful to all who have supported me along the way. This thesis is completely for you since, without your help, this achievement would not have been possible.

邵欣圓

Xinyuan Shao
May 2025, Gothenburg

致谢

此博士论文集中包含我于 2021 到 2025 年间在瑞典查尔姆斯理工大学的研究工作。四年的学习生涯匆匆而过。时间好似只是穿过我，但无形中在我身上和心里留下印记。经年之后，这段记忆可能会变得模糊，可是此时此刻，我满心感激。

在这里，我首先想要感谢我的导师，Jonas Ringsberg 教授。谢谢您在四年间给我的鼓励和无条件的支持。我从您身上看到了尽职尽责的工作态度和对研究的无尽热情。我也将会把它们带到我未来的工作生活中。

我想感谢我的合作导师们，姚华栋教授，李志远教授和 Erland Johnson 教授。感谢你们对我一直以来的指导和支持。在跟你们的每一次交流讨论中我都学到了很多。由衷感谢姚老师，从硕士毕设开始，您给我的指导，指引和支持让我受益良多。良师益友莫如是！

我想感谢我身边的所有朋友们。我的快乐和悲伤都有你们与我分享和分担。特别感谢在 18-19 年我在北京结识的朋友们，虽然匆匆相逢又匆匆别过，但你们的陪伴和支持让我在北京的时间里并不孤单。由衷感谢我的朋友肖荷喆同她的丈夫肖道儒，和蔡瑶以及她的猫咪李亚 Lyapunov。你们时时刻刻都用你们的方式来支持我，并且总是以充足的耐心聆听我。非常感谢！

我想谢谢我的爸爸妈妈妹妹和弟弟。你们总是默默支持我的各种决定，给我全力的协助。我非常感激。

感谢所有的合作者和所有帮助过我的人，你们的无私与耐心曾经照亮了我。也感谢出现在我生活中给我带来烦恼的人和事，我因为你们变得更加包容平和。

感谢国家留学基金委和我的母校南京航空航天大学。2016 年我在南航拿到了优秀本科生交流奖学金来瑞典做交换生，这才与瑞典结缘。一晃九年已经过去了，没有当时的开始，我绝不会在之后选择在瑞典继续硕博的学业。谢谢。

感谢瑞典查尔姆斯理工大学给予我的培养支持和平等的机会。六年间我长了知识和见识，认识了同事朋友和导师，从二十出头到快三十，这些全都在这所学校发生。感谢六年来学校对我的栽培和尊重。

我也想谢谢我自己，谢谢你的坚持和从头开始的勇气。从 2019 年至今，在瑞典的六年里，在足够长的独处的时间里，我审视自己，除了学术知识，我也学会了如何应对各种挫折并且找到内心的平静。

最后，我感谢这一路上所有的经历，感谢上天赐予我健康，头脑，机遇，良师，益友和家人。我希望自己在接下来的工作和生活中能够更加坚强和坚韧，淡定和淡然，永葆一颗平常心，享受生命。不管未来我在何种领域从事何种工作，我都希望自己脚踏实地实事求是，尽力而为问心无愧。这些体悟是读博经历给予我的比知识更重要的东西。自勉。

邵欣圆

2025 年 5 月

Contents

List of appended papers

This thesis is based on the following publications:

[A] **Shao, X.**, Yao, H.-D., Ringsberg, J. W., Li, Z., & Johnson, E. (2024). Performance analysis of two generations of heaving point absorber WECs in farms of hexagon-shaped array layouts. *Ships and Offshore Structures*, 19(6), 687-698.

[B] **Shao, X.**, Ringsberg, J. W., Yao, H.-D., Li, Z., Johnson, E., & Fredriksson, G. (2023). A comparison of two wave energy converters' power performance and mooring fatigue characteristics – One WEC vs many WECs in a wave park with interaction effects. *Journal of Ocean Engineering and Science*, 8(4), 446-460.

[C] **Shao, X.**, Ringsberg, J. W., Yao, H.-D., Gowda, U. R. S. L., Khedkar, H. N., & Todalshaug, J. H. (2024). Hydrodynamic interactions and enhanced energy harnessing amongst many WEC Units in large-size wave parks. *Journal of Marine Science and Engineering*, 12(5), 730.

[D] **Shao, X.**, Ringsberg, J. W., Johnson, E., Li, Z., Yao, H.-D., Skjoldhammer, J. G., & Björklund, S. (2025). An FMI-based co-simulation framework for simulations of wave energy converter systems. *Energy Conversion and Management*, 323, 119220.

[E] **Shao, X.**, Forsberg, J., & Ringsberg, J. W. (2025). Integrating detailed power take-off system models in wave energy converter simulations using an FMI-based co-simulation approach. *Ocean Engineering*, 335, 121651.

List of other papers

Other publications by the author not included in this thesis:

[1] **Shao, X.**, Folkow, P. D., & Eskandari-Ghadi, M. (2021). The closest isotropic, cubic and transversely isotropic stiffness and compliance tensor to an arbitrary anisotropic material. *Journal of Mechanics of Materials and Structures*, 16(4), 451-470.

[2] **Shao, X.**, Santasmasas, M. C., Xue, X., Niu, J., Davidson, L., Revell, A. J., & Yao, H.-D. (2022). Near-wall modeling of forests for atmosphere boundary layers using lattice Boltzmann method on GPU. *Engineering Application of Computational Fluid Mechanics*, 16(1), 2143-2156.

[3] **Shao, X.**, Yao, H.-D., Ringsberg, J. W., Li, Z., & Johnson, E. (2022). Performance analysis of two generations of heaving point absorber WECs in farms of hexagon-shaped array layouts. *Proceedings of The 7th International Conference on Ships and Offshore Structures (ICSOS 2022), 17-18 October 2022, Ålesund, Norway*, 183-195.

[4] **Shao, X.**, Yao, H.-D., Ringsberg, J. W., Li, Z., Johnson, E., & Fredrikson, G. (2022). A comparison of the performance and characteristics of two generations Waves4Power WaveEL wave energy converters. *Proceedings of The 5th International Conference on Renewable Energies Offshore (RENEW 2022), 8-10 November 2022, Lisbon, Portugal*, 277-284.

[5] **Shao, X.**, Ringsberg, J. W., Yao, H.-D., Li, Z., & Johnson, E. (2023). Fatigue of mooring lines in wave energy parks. *Advances in the Analysis and Design of Marine Structures - Proceedings of the 9th International Conference on Marine Structures (MARSTRUCT 2023), 3-5 April 2023, Göteborg, Sweden*, 205-211.

[6] **Shao, X.**, Yao, H.-D., Ringsberg, J. W., Skjöldhammer, J. G., & Lin, J. (2023). FSI simulations and analyses of a non-resonant buoyant wave energy converter. *Proceedings of the International Conference on Ocean, Offshore and Arctic Engineering (OMAE 2023), 11-16 June 2023, Melbourne, Australia*, Vol. 8, V008T09A063.

[7] **Shao, X.**, Ringsberg, J. W., Yao, H.-D., Johnson, E., Forsberg, J., Zeinali, S., Lindström, J., & Wiktorsson, M. (2024). A comparison of approaches integrating power take-off systems into wave energy converters simulations. *Proceedings of the 6th International Conference on Renewable Energies Offshore (RENEW 2024), 19-21 November 2024, Lisbon, Portugal*, 351-358.

Acronyms

BEM	Boundary Element Method
DoF	Degree-of-Freedom
CFD	Computational Fluid Dynamics
EC	Environmental Condition
FMI	Functional Mock-up Interface
FMU	Functional Mock-up Unit
HIL	Hardware-In-the-Loop
LCoE	Levelized Cost of Energy
LPF	Linear Potential Flow model
N-S	Navier-Stokes
OWC	Oscillating Water Column
PTO	Power Take-Off
RFC	RainFlow Counting
RMSE	Root Mean Square Error
RN	Relative tension-Number of cycles to failure
TRL	Technological Readiness Level
WEC	Wave Energy Converter

Mathematical symbols

Greek notations

α	Intercept parameter of the RN curve [-]
γ_F	Safety factor [-]
$\varphi_{r,j}$	Radiated potential of unit oscillation in the j-th DoF [m]
ϕ	Velocity potential [m^2/s]

ϕ_D	Incident potential [m^2/s]
ϕ_I	Diffracted potential [m^2/s]
ϕ_R	Radiated potential [m^2/s]
ρ	Mass density [kg/m^3]
ω	Wave frequency [rad/s]

Latin notations

$\mathbf{A}(\omega)$	Frequency-dependent added mass matrix [kg]
$\mathbf{A}\|_{\omega=\infty}$	Added mass matrix at infinite wave frequency [kg]
$\mathbf{B}(\omega)$	Frequency-dependent radiation damping matrix [kNs/m]
B_{PTO}	PTO damping [kNs/m]
D	Mooring line fatigue damage [-]
$\mathbf{F}_{\text{excitation}}$	Wave excitation force vector [N]
$\mathbf{F}_{\text{mooring}}$	Mooring force vector [N]
$\mathbf{F}_{\text{other}}$	Other force vector [N]
$\mathbf{F}_{\text{PTO}}$	Power take-off force vector [N]
$\mathbf{F}_{\text{radiation}}$	Radiation force vector [N]
g	Acceleration of gravity [m/s^2]
$\mathbf{h}$	Acceleration impulse response function [kg/s]
H	Heaviside function [-]
H_s	Significant wave height [m]
K_{PTO}	PTO stiffness [N/m]
$\mathbf{M}$	Mass matrix [kg]
$\mathbf{n}$	Normal vector of body surface [-]
p	Pressure [Pa]
P_{LD}	Power performance of linear-damper PTO system model [kW]
R_i	Relative tension cycle [-]

t	Time [s]
T	Simulated physical time [s]
T_p	Peak period [s]
$\dot{x}$	Velocity [m/s]
$\ddot{x}$	Acceleration [m/s^2]
$\dot{\mathbf{X}}$	Velocity vector [m/s]
$\ddot{\mathbf{X}}$	Acceleration vector [m/s^2]
z	Vertical position coordinate [m]
z_{es}	End-stop stroke [m]

CHAPTER 1

Introduction

Humans have a constant need for energy to sustain their lives. From primitive humans' use of wood to conventional energy sources like oil and natural gas, more stable and efficient energy sources have been humanity's eternal quest. Since the beginning of the 21st century, environmental friendliness and sustainability have been added as critical dimensions when evaluating energy sources (International Renewable Energy Agency, 2019; United Nations, 2012; World Wide Fund for Nature, 2023). Renewable energy is expected to help meet the environmental, economic, and social challenges associated with conventional energy sources while enhancing the EU's industrial competitiveness (European Commission, 2025). Other countries beyond Europe are also transitioning towards renewable energy. Many developing nations are leveraging renewables to bypass traditional fossil-fuel-based infrastructures and strengthen energy security. Among the many types of renewable energy, wave energy has attracted attention in the global market and from the research community due to its abundance and around-the-clock availability.

1.1 Background and motivation

Renewable energy includes energy sources that are naturally replenished and sustainable over time. Solar, wind, and wave are three representative energy sources from the renewable energy family. The first two have been broadly commercialised and are now among the most widely deployed renewable energy sources globally. Their extraction technologies are mature and standardised. Solar photovoltaic technology

is a successfully commercialised form of solar energy (El Hammoumi et al., 2022; Kabir et al., 2018), while onshore and offshore wind turbines extract large amounts of wind energy (Kaldellis & Apostolou, 2017). As of 2022, solar and wind energy each provided 1% of the total world energy supply, and they are expected to contribute 3% each to the total world energy supply by 2030 (International Energy Agency, 2023).

Wave energy has many advantages over solar and wind energy, among which is its high power density. The process by which energy is transferred from solar to wind to waves naturally concentrates it. Wind arises from the movement of the air due to its uneven heating by the sun. As the wind blows across the ocean, it transfers energy to the water, generating waves. Through this process, the energy intensity increases from 0.1-0.3 kW/m^2 on a flat horizontal surface receiving solar radiation, to 0.5 kW/m^2 perpendicular to wind direction, then finally to 2-3 kW/m^2 perpendicular to the wave's incoming direction (Falnes, 2007). Besides its high power density, wave energy also features continuous availability around the clock, unlike solar energy. With these advantages, wave energy has aroused high expectations on the part of the public and is an important complement to other renewable energy sources.

Attempts to harness wave energy can be traced back to 1799 in Paris, when Pierre-Simon and his son filed the first patent for wave energy extraction (Falcão, 2010). In modern times, the rise of comprehensive research on wave energy extraction technologies began with the first oil crisis. Increasing oil prices impelled governments and research communities to find alternative energy sources. Ironically, the price of oil influenced the financial support for wave energy extraction technology, as with a drop in oil prices in the 1980s, interest in wave energy also declined. It was not until 1994, with the Fourth Framework Programme of the European Community, that wave energy returned to centre stage in the research community (Polinder & Scuotto, 2005). Wave energy extraction technologies have since been under development with governmental support in many countries with abundant wave energy resources, such as Denmark, Ireland, Norway, Portugal, Sweden, and the UK (Clément et al., 2002).

However, even after over 50 years of development since the first oil crisis in the 1970s, wave energy still has a long way to go to achieve full commercialisation (Ahamed et al., 2020; Jin & Greaves, 2021; Sheng, 2019). This is due to multi-fold reasons besides shifting research interests and lack of funding.

The devices that extract wave energy are called wave energy converters (WECs). Unlike solar panels and wind turbines, which have a unified shape and working principle, WECs vary significantly in design. According to the classification by Falcão (2010), WECs can be generally classified based on their working principles into oscillating water columns (OWCs), oscillating bodies, and overtopping devices. Regarding the mobility of WECs, each subcategory can be further divided into floating, fixed, and submerged structures (Falcão, 2010). Despite the numerous classifications, each type can be matched with corresponding projects that have reached at least the pro-

totype stage. The decentralisation of WEC designs has caused a dispersal of research funding and aggravates the difficulty of sharing research findings (López et al., 2013).

From an energy conversion perspective, WECs must convert irregular mechanical motions into electricity, which is less straightforward and efficient than in conventional coal-burning power stations and other renewable energy sources like solar panels and wind turbines (Sheng, 2019). The power take-off (PTO) system must be carefully designed to achieve steady energy conversion. Based on their working principles, PTO systems can be classified into many groups, such as hydraulic motor systems, pneumatic air turbine transfer systems, hydro turbine transfer systems, direct mechanical drive systems, direct linear electrical drive systems, and hybrid systems (Ahamed et al., 2020). As a core subsystem of the WEC, the PTO system is deeply coupled with other subsystems, for example, the hydrodynamical system, including the buoy; the mechanical system, including joint connections; and the mooring system, usually consisting of multiple mooring lines and floaters. The couplings introduce complexity into WEC designs, making detailed experiments and numerical simulations necessary during the WEC development processes.

From an economic perspective, the levelized cost of energy (LCoE) of WECs should be minimised to compete with other energy sources and achieve full commercialisation of wave energy (Chang et al., 2018; De Castro et al., 2024; Guo et al., 2021). Otherwise, wave energy will never be competitive in the global market. There is consensus that one way to lower the LCoE is to deploy multiple WECs in proximity to form a wave park (Giassi et al., 2020; Teixeira-Duarte et al., 2022; Têtu & Fernandez Chozas, 2021). The total cost can be reduced by sharing mooring lines, power cables, and anchors (Shao et al., 2024). However, when multiple WECs are deployed in proximity, the waves diffracted and radiated by the WECs interfere with the incoming wave, resulting in complex wave fields (Liu et al., 2022; Zou et al., 2024). The interaction effects, including diffraction and radiation, can propagate within the entire wave field and affect the power performance of all WECs (Babarit, 2013; Borgarino et al., 2012; Yang et al., 2020). Moreover, the coupling of each subsystem within the WEC is superimposed upon the interaction effects, making the wave park design more complex and uncertain.

Physical experiments involving a single WEC are costly, to say nothing of wave parks. The diversity of WEC designs hinders the possibility of joint experiments from multiple cooperators, while the deeply coupled subsystems make the results of simplified or decoupled experiments questionable. Therefore, numerical simulations constitute a good alternative, especially during the design phase of a single WEC or wave park, when fast-paced iterations are required; however, they also face certain challenges. The coupling of each subsystem within a WEC can hardly be included in simulations using commercial software such as Ansys Aqwa (Ansys, Inc., 2025a), DNV SESAM (DNV, 2025b) and OrcaFlex (Orcina, 2025), which were initially designed for ship and offshore platform simulations. By coupling different tools and

solvers, the limitations of a single software may be overcome. However, new issues, such as the communication between different solvers, then arise. A numerical simulation framework covering different simulation goals ranging from general power estimation to the detailed analysis of each subsystem of single WECs and wave parks would be of great value to the wave energy community.

The primary motivation of this thesis is to resolve the challenges in developing single WECs and wave parks using numerical simulation approaches. The research topics include the numerical modelling of single WECs and wave parks, the analysis of power estimation and mooring fatigue damage, and an investigation of interaction effects in different wave park layouts. More generally, this thesis intends to introduce a comprehensive numerical simulation framework that can integrate the subsystem models of a WEC system and enable a detailed global simulation, which is expected to yield more accurate and thorough results to guide the design of single WECs and wave parks.

1.2 Objectives and goals

The main objective of this thesis is to develop numerical frameworks for modelling, power performance estimation, and mooring fatigue damage evaluation for single WECs and wave parks. The model within the proposed numerical framework is designed to be easily implemented and flexible enough to accommodate different simulation goals, ranging from general power estimations to detailed subsystem analyses. The main objective of this thesis comprises several incremental goals:

- **G1:** Build numerical models of different WEC prototypes, whether as a single WEC or in a wave park, within a numerical framework based on a single commercial software. Identify the gap between the simulation goals and the limitations of the chosen commercial software.

- **G2:** Propose a new numerical framework that seamlessly integrates multiple solvers and tools to enable more comprehensive and accurate WEC system modelling and facilitate multidisciplinary collaboration in the industry.

- **G3:** Investigate the interaction effects of wave park layouts with different WEC concepts. Systematically evaluate the power performance and mooring fatigue damage to demonstrate the capability of the numerical frameworks.

- **G4:** Integrate a detailed PTO system model into global simulations of single WECs and wave parks. Compare results from models with PTO system models of different fidelity levels. Understand the influence of the fidelity level of a subsystem model on the overall global simulation results.

1.3 Assumptions and limitations

The theoretical foundation of the adopted hydrodynamic solvers is based on linear potential theory. Potential theory assumes that the fluid is incompressible and inviscid and that the flow is irrotational. The linearisation assumes that the wave amplitude is small compared to the wavelength and water depth and that the boundary conditions are linearised to the static water level. Several restrictions must be imposed to ensure that these assumptions are valid: the body size and motion should be small relative to the wavelength and wave height; the body should not deform largely under wave loads; and the free surface elevation should be small enough that the linearised free surface boundary condition holds.

Accordingly, in this thesis, the WEC bodies are assumed to be rigid, and structural deformations are neglected. The power cables which transfer electricity from the WECs to substations and grids are not included in the simulation cases. The simulated wave conditions are limited to linear waves; nonlinear effects such as wave breaking and vortex shedding are excluded. Wind and current loads are not considered, and the effects of biofouling are not investigated. In some cases, viscous forces are accounted for using drag coefficients derived from experimental data and practical experience. The hydrostatic force is calculated on the instantaneous wetted surface to partially capture the nonlinear wave loads caused by the body's large motion.

In addition to the limitations due to the assumption of linear potential theory, the simulations of the individual WECs and wave parks in this thesis generally lack thorough experimental validations. Although a comparison between the numerical model and a benchmark study has been conducted to validate the proposed numerical frameworks, real full-scale experimental data are still unavailable. Therefore, this thesis demonstrates the proposed numerical frameworks and their capabilities in simulating single WECs and wave parks with a variety of working principles. The lack of experimental validation does not negate the practicability of the proposed numerical frameworks. Instead, if experimental data are available in the future, the numerical models can be calibrated and fine-tuned to represent the physical WEC prototypes more accurately.

1.4 Thesis outline

The outline of the remaining chapters is as follows: The methodology applied in this thesis is described in Chapter 2. The numerical models for the three WEC prototypes are introduced in detail in Chapter 3. The verification and validation of the numerical framework are provided in Chapter 4. Chapter 5 gives summaries of the five appended papers. Chapter 6 discusses some aspects based on the results. Chapter 7 concludes with a discussion of the main contributions of this thesis. Chapter 8 adduces some issues for possible future study.

CHAPTER 2

Methodology

This chapter introduces the methods used in this thesis, from numerical methods to data post-processing.

2.1 Loads on WECs

A WEC system's motion response results from all the forces/moments acting on the WEC. According to Newton's Second Law, the net force exerted on a body equals the product of its mass and acceleration. Applying this to a 6 Degree-of-Freedoms (DoFs) WEC system under sea loads with PTO and mooring systems and assuming the WEC is a single body yields:

$$\mathbf{M}\ddot{\mathbf{X}} = \mathbf{F}_{\text{hydro}} + \mathbf{F}_{\text{PTO}} + \mathbf{F}_{\text{mooring}} + \mathbf{F}_{\text{other}}, \tag{2.1}$$

where the terms on the left- and right-hand sides are defined as follows:

- $\mathbf{M}$ is the 6×6 mass matrix of the bodies.
- $\ddot{\mathbf{X}}$ is the 6×1 acceleration matrix of the bodies.
- $\mathbf{F}_{\text{hydro}}$ is a 6×1 vector, which is the sum of the hydrodynamic and hydrostatic loads.
- $\mathbf{F}_{\text{PTO}}$ is a 6×1 vector, representing the force from the PTO system.
- $\mathbf{F}_{\text{mooring}}$ is a 6×1 vector, representing the station-keeping force from the mooring system.

- $\mathbf{F}_{\text{other}}$ is a 6×1 vector, which includes all other forces, such as the wind and current loads and the forces from the additional damping and stiffness of the inner components in the WEC system.

A schematic diagram of the application of this force analysis to a WEC system is shown in Fig. 2.4. Each force term should be accurately evaluated to adequately solve for the WEC's motion and estimate its power performance.

2.2 Linear potential theory and boundary element method

A theory widely used in ocean engineering is the linear potential theory, which is derived from potential theory with certain linearisations. The fundamental equation of potential theory is the Laplace equation:

$$\nabla^2 \phi = 0, \tag{2.2}$$

where ϕ is the velocity potential. Compared to the Navier-Stokes (N-S) equations, the Laplace equation is based on two main assumptions: the fluid is incompressible and inviscid, and the flow is irrotational. These assumptions reduce the three-component velocity vector in the N-S equations to a single velocity potential in the Laplace equation, significantly simplifying computations.

The linearisations applied in linear potential theory are twofold. First, the boundary conditions are linearised by ignoring second-order terms and by being applied to the system in static equilibrium. Second, the velocity potential is divided into three independent parts: the incident, diffracted, and radiated potentials (ϕ_I, ϕ_D, and ϕ_R). Specifically, the radiation potential can be further divided so as to be proportional to the oscillation velocity in each DoF. Therefore, the velocity potential can be written as:

$$\phi = \phi_I + \phi_D + \underbrace{\sum_{j=1}^{6} \varphi_{r,j} \dot{x}_j}_{\phi_R}, \tag{2.3}$$

where j refers to the j-th DoF, $\dot{x}_j$ is the velocity in the j-th DoF, and $\varphi_{r,j}$ is the radiated potential caused by a unit oscillation velocity in the j-th DoF. Each potential can be solved separately by substituting it into the Laplace equation and applying the appropriate boundary conditions. Thus, the total force exerted on the body can be divided into hydrostatic force, wave excitation force, and radiation force.

The boundary element method (BEM) is widely employed to solve the velocity potential in the Laplace equation in the frequency domain for various wave frequencies ω. Many solvers have adopted BEM, such as WAMIT (WAMIT, Inc., 2025), Ansys Aqwa (Ansys, Inc., 2025a), HydroD (DNV, 2025a), and NEHOM (Ecole Centrale de

Nantes, 2025). After solving for the velocity potential, the pressure acting on the body surface can be calculated as:

$$p = -\rho g z - \rho \frac{\partial \phi}{\partial t}, \tag{2.4}$$

where g is the acceleration of gravity, z is the vertical position coordinate and ρ is the density. The force $\mathbf{F}_{\text{hydro}}$ is obtained by integrating the pressure of the wetted surface:

$$\mathbf{F}_{\text{hydro}} = -\iint_{S_w} p\mathbf{n} dS, \tag{2.5}$$

where $\mathbf{n}$ is the normal vector of the body surface. $\mathbf{F}_{\text{hydro}}$ may be divided into three components:

$$\mathbf{F}_{\text{hydro}} = \mathbf{F}_{\text{hydrostatic}} + \mathbf{F}_{\text{excitation}} + \mathbf{F}_{\text{radiation}}. \tag{2.6}$$

$\mathbf{F}_{\text{hydrostatic}}$ is the hydrostatic force, which can be calculated using the instantaneous wetted surface to increase accuracy. $\mathbf{F}_{\text{excitation}}$ is the wave excitation force caused by the incident and diffracted waves, assuming that the body is fixed. Finally, $\mathbf{F}_{\text{radiation}}$ is the radiation force caused by the radiated waves, assuming that the body oscillates in calm water. $\mathbf{F}_{\text{radiation}}$ can be rewritten using the acceleration and velocity of the body:

$$\mathbf{F}_{\text{radiation}} = -\mathbf{A}\ddot{\mathbf{X}} - \mathbf{B}\dot{\mathbf{X}}, \tag{2.7}$$

where $\mathbf{A}$ and $\mathbf{B}$ are the frequency-dependent added mass and radiation damping matrices, each of dimension 6×6, calculated from the radiated velocity potential. For detailed theoretical derivations, one can refer to the textbook by Newman (2017) and the paper by Papillon et al. (2020). The values of the added mass and radiation damping are provided by BEM solvers.

2.3 Equation of motion in the time domain

The Laplace equation is usually solved in the frequency domain, where the waves are assumed to be sinusoidal with frequency ω to simplify the computation. The added mass and radiation damping are thus frequency dependent. However, in a real physical situation where the waves are irregular and the forces from PTO and mooring systems are time-dependent, time-domain analyses are inevitable.

The expression for $\mathbf{F}_{\text{radiation}}$ in the time domain, derived by Cummins et al. (1962), is:

$$\mathbf{F}_{\text{radiation}} = -\mathbf{A}|_{\omega=\infty}\ddot{\mathbf{X}} - \int_0^t \mathbf{h}(t-\tau)\,\ddot{\mathbf{X}}(\tau)\,d\tau, \tag{2.8}$$

where $\mathbf{A}|_{\omega=\infty}$ is the radiation mass matrix at infinite wave frequency and $\mathbf{h}$ is the acceleration impulse response function. $\mathbf{h}$ can be calculated using the radiation

damping as:

$$\mathbf{h}(t) = \frac{2}{\pi}\int_0^\infty \mathbf{B}(\omega)\frac{\sin(\omega t)}{\omega}d\omega. \tag{2.9}$$

The wave excitation force $\mathbf{F}_{\text{excitation}}$ in the time domain is computed by summing up all the excitation forces of the different wave components. The hydrostatic force $\mathbf{F}_{\text{hydrostatic}}$ can be computed either by assuming a constant hydrostatic matrix based on the equilibrium position or, for higher accuracy, by integrating the hydrostatic pressure over the transient wetted surface.

By substituting all the forces in the time domain and rearranging Eq. (2.1), the equation of motion in the time domain can be written as:

$$\begin{aligned}(\mathbf{M} + \mathbf{A}|_{\omega=\infty})\ddot{\mathbf{X}} = -\int_0^t \mathbf{h}(t-\tau)\ddot{\mathbf{X}}(\tau)\,d\tau \\ +\mathbf{F}_{\text{hydrostatic}} + \mathbf{F}_{\text{excitation}} + \mathbf{F}_{\text{mooring}} + \mathbf{F}_{\text{PTO}} + \mathbf{F}_{\text{other}},\end{aligned} \tag{2.10}$$

which is the fundamental equation in WEC system analysis.

2.4 Hydrodynamic interaction effects

Hydrodynamic interaction effects in this thesis refer to the interference caused by neighbouring WECs on incoming waves when multiple WECs are installed in a specific area to form a wave park. These effects include diffraction and radiation. The resulting changes in the wave field ultimately affect WEC motions and power performance. The velocity potential of a wave park consisting of M WECs can be written as:

$$\phi = \phi_I + \phi_D + \underbrace{\sum_{m=1}^{M}\sum_{j=1}^{6}\varphi_{r,jm}\dot{x}_{jm}}_{\phi_R}, \tag{2.11}$$

where $\varphi_{r,jm}$ is the radiated potential caused by a unit oscillation velocity of the m-th body in the j-th DoF. ϕ_D includes the interaction effects as long as proper boundary conditions are applied. Compared to single-WEC cases, the number of DoFs in cases with multiple WECs increases from 6 to $6M$, where M is the total number of WECs.

2.5 Fatigue damage analysis of the mooring lines

The accumulated fatigue damage of the mooring lines is an important factor in the evaluation of a mooring system and the overall WEC system design from an LCoE perspective. According to DNV standards (DNV, 2021), for fibre ropes, the relative tension-number of cycles to failure (RN) approach should be applied to estimate the accumulated mooring fatigue damage. The mooring fatigue damage may be

estimated as:

$$D = \sum_i \frac{R_i^m}{\alpha} \cdot \gamma_F, \tag{2.12}$$

where i stands for the i-th relative tension cycle identified by the rainflow counting (RFC) method, R_i is the relative tension range of each cycle, and m and α are two constant parameters; the values of m and α recommended by the DNV standards are 13.46 and 0.259, respectively. Finally, γ_F is the safety factor, whose value is taken to be 60 for a larger safety margin and to cover a range of uncertainties in the fatigue analysis according to DNV standards (DNV, 2021).

2.6 Power performance analysis

The power performance estimation of a WEC is relevant to its working principle and the modelling approach of its PTO system. The WEC prototypes studied in this thesis are point-absorbers extracting wave energy from the heaving motion of the WECs.

For a simplified PTO model which uses a linear damper with damping coefficient B_{PTO} and assumes that energy is only extracted from the vertical heaving motion, the time-averaged power performance P_{LD} can be calculated as:

$$P_{LD} = \frac{1}{T} \int_0^t B_{PTO} \dot{z}^2 dt, \tag{2.13}$$

where T is the total simulation duration and $\dot{z}$ is the heaving velocity. The criteria for choosing B_{PTO} vary for specific WEC prototypes.

Suppose the PTO system is modelled by considering its subcomponents, such as hydraulic cylinders, accumulators, and generators. In that case, the power performance estimation will depend on the specific PTO system modelling approaches. In Section 3.1.3, a detailed PTO system model for WaveEL WEC is given and the power performance estimation for that specific PTO system model is discussed there. The PTO system model is case-specific for different WEC prototypes.

2.7 Numerical simulation frameworks

A WEC system combines all the subsystems, such as the hydrodynamic, mechanical, PTO, and mooring systems. Each subsystem must be modelled individually and combined into a global model for realistic power performance estimation and mooring fatigue analysis. In this thesis, the term numerical framework explicitly denotes the computational structure designed to model WEC systems, incorporating multiple numerical approaches to simulate coupled hydrodynamic, structural, and control interactions. Mature and standardised numerical frameworks must be established and

adopted for WEC designs and development to facilitate fast modelling and simulation processes. Two numerical simulation frameworks are adopted in this thesis to achieve global simulations of single WEC systems and wave parks with different fidelity levels.

2.7.1 DNV SESAM framework

The DNV SESAM framework refers to the numerical framework based on the DNV SESAM software package, which contains many tools and programs for hydrodynamic and structural analyses of ships and offshore structures (DNV, 2025b). As shown in Fig. 2.1, the tools used in the so-called DNV SESAM framework in this thesis are GeniE (GeniE, 2025), HydroD (DNV, 2025a), and Sima (Sima, 2025). GeniE is for geometry modelling and panel discretisation, which provides inputs for the BEM solver Wadam in HydroD. Sima is a time-domain analysis tool in which Simo solves the equation of motion, and Riflex solves the mooring forces based on the instantaneous motions of the body. Simo and Riflex are fully coupled, which means that body motions and mooring forces influence each other mutually at each time step during the simulations. According to Yang et al. (2016), fully coupled simulations can better capture the interaction between the components of a WEC system and give more accurate results than decoupled simulations.

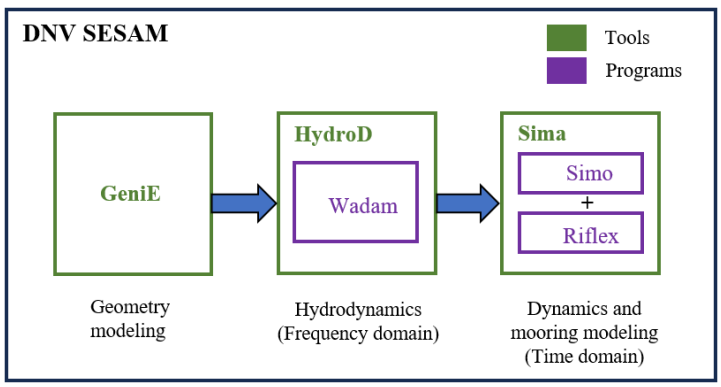

Figure 2.1: The tools and programs in the DNV SESAM software involved in the DNV SESAM framework in this thesis, from **Paper A**.

The theories behind each program are shown in Fig. 2.2. Wadam solves the added mass, radiation damping, and wave excitation force transfer functions in the frequency domain using BEM. In Sima, the frequency-dependent hydrodynamic coefficients are transferred into the time domain through impulse response functions. Other forces, such as the PTO force and mooring force, can also be added to Sima. The program Simo in Sima solves the equation of motions in the time domain and gives the results for the WEC motions and mooring forces. Readers can find ex-

amples of models built under the DNV SESAM framework in the appended **Paper A-C**.

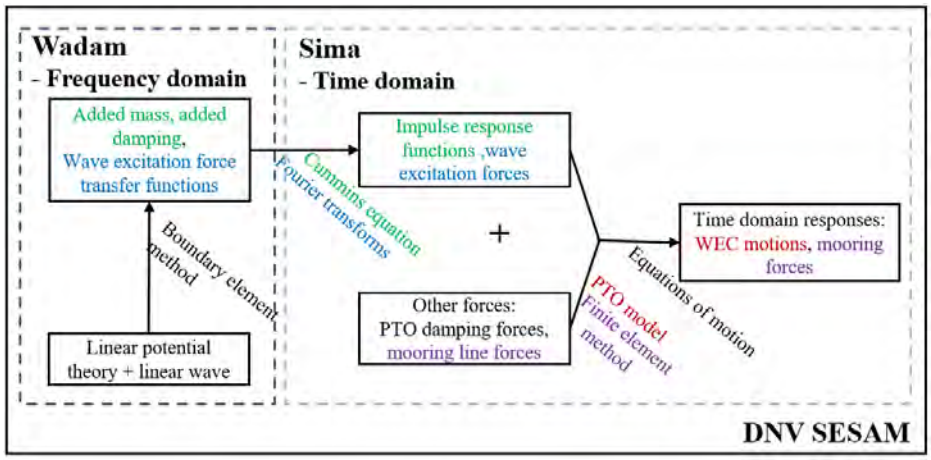

Figure 2.2: DNV SESAM theoretical framework, from Shao (2023).

2.7.2 FMI-based co-simulation framework

The term co-simulation generally applies to simulations that couple different solvers, each responsible for a specific subsystem, with communication between solvers to exchange data at defined intervals. This allows each solver to use its own numerical methods and time-stepping approach while ensuring system-wide interaction. Many approaches have been applied to handle communication between the solvers. For example, the co-simulation in Bulian and Cercos-Pita (2018) is enabled through an in-house communication tool based on Transmission Control Protocol/Internet Protocol (TCP/IP) connections, while the co-simulation in Dang et al. (2020) is achieved by integrating an in-house 6-DoF rigid-body dynamics solver into Ansys Fluent as a user-defined function (UDF). Moreover, the approach in Jiao et al. (2024) employs the SIMULIA co-simulation engine. These examples demonstrate the diversity of co-simulation implementations.

However, in this thesis, co-simulation specifically refers to functional mock-up interface (FMI)-based co-simulation. FMI is a standard first developed under the Modelisar project (ITEA4, 2025). It defines the interface between numerical models and simulation environments, enabling tool-independent communication among solvers (Modelica Association, 2025). The models built by different software or self-written programs can be encapsulated into functional mock-up units (FMUs) following FMI standards and coupled with each other via an FMU-supported platform to form global FMI-based co-simulations.

Fig. 2.3a illustrates the architecture of a general FMI-based co-simulation. It is worth noting that the co-simulation algorithm is not a part of the FMI standard but is instead provided by FMU-supported platforms like Dymola (Dassault Systèmes, 2025), Ansys Twin Builder (Ansys, Inc., 2025b), and Simulink (MathWorks, 2025). The main functions of a co-simulation algorithm are advancing the simulation time and exchanging data between FMUs. Many commercial software packages, such as the software used in this thesis, Ansys Aqwa and Ansys Rigid Dynamics, support FMI standards and can export simulation models into FMUs. Fig. 2.3b shows an example FMU exported by Ansys Aqwa. Modelling details are encapsulated, while inputs and outputs are standardised pins. A global co-simulation can quickly be established by adequately connecting the input and output pins of different FMUs without explicit programs written for data communications.

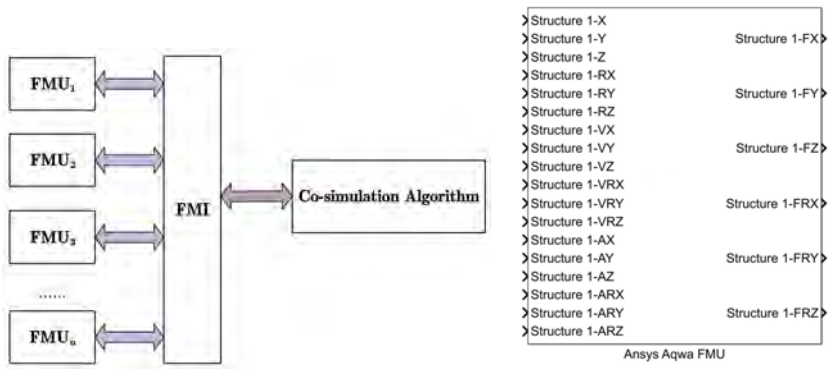

Figure 2.3: (a) Diagram of a general FMI-based co-simulation model, (b) an example of an FMU exported by Ansys Aqwa. Both are from **Paper D**.

Fig. 2.4 shows an FMI-based co-simulation model for an example WEC system. The hydrodynamic and mooring system is modelled in Ansys Aqwa, while the mechanical system is modelled in Ansys Rigid Dynamics. The PTO system model, which can be either a linear damper or a detailed model, is directly modelled in Simulink. For more examples of FMI-based co-simulations, the reader can refer to cases in the appended **Paper D** and **E**.

2.7.3 Comparison of two numerical frameworks

The ultimate goal of the two numerical frameworks in this thesis is the same: to model a WEC system with the effects from all subsystems and provide realistic estimations of power performance and mooring fatigue damage. However, from the perspectives of modelling convenience and model fidelity level, the two have significant differences.

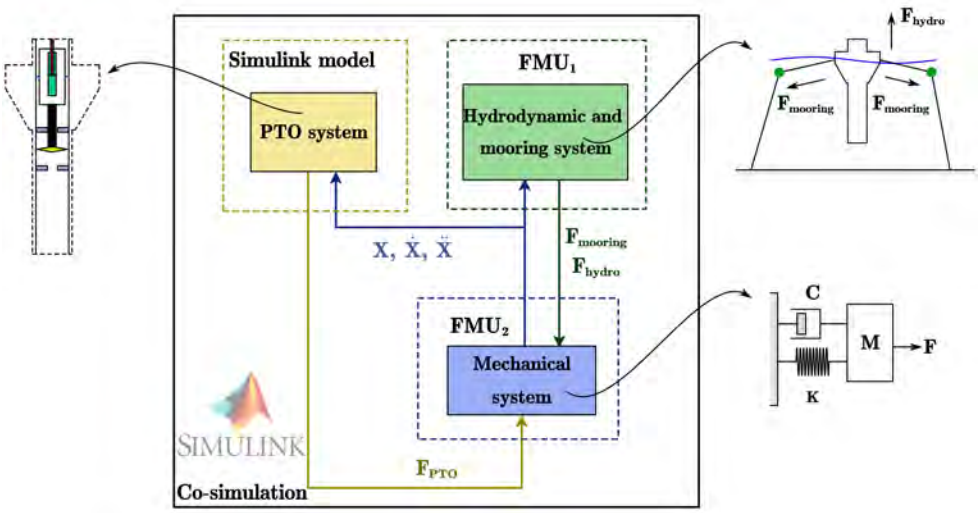

Figure 2.4: FMI-based co-simulation framework for an example WEC system, adopted from **Paper E**.

The DNV SESAM software package provides an integrated simulation environment in which the time-domain model of a WEC system can be directly built. However, the side-effect of the integration is the rigidity of the modelling. DNV SESAM is not good at modelling multibody dynamics and detailed PTO systems due to the limited functions and tools available in the software package. Therefore, for WECs modelled using DNV SESAM, the PTO system is usually simplified as a linear damper, as seen in the series of studies by Ringsberg et al. (2020a) and Yang et al. (2016, 2017b, 2017a, 2020), which in many situations is far from reality. Even though the simplification may be acceptable in certain respects, its impact on power performance and mooring fatigue damage predictions remains unclear.

Moreover, DNV SESAM is not capable of adequately modelling joint connections between different WEC components, which are present in many WEC prototypes, such as raft-type WECs (Shi et al., 2021; Zhang et al., 2023), bean-shaped WECs (Sricharan & Chandrasekaran, 2021), and WECs connected to offshore wind turbines (Ghafari et al., 2022; Wei et al., 2024), ships (Gu et al., 2023), or floating platforms (He et al., 2023) through hinges.

The mechanical systems within WECs can be even more complicated than joints. They influence the motion patterns of WECs, affecting the power performance. For example, the SJTU-WEC uses a 4-bar and spherical linkage to convert motions into reciprocating rotation (Chen et al., 2021). The PUWEC uses prismatic pairs in its hydraulic cylinder and universal pairs in its gear transmission system (Bao et al., 2023). The MDWEC uses six parallel hydraulic cylinders to extract energy from a

moving buoy (Gao et al., 2024). The 'rolling' WEC uses a mechanical motion rectifier (MMR) PTO system to achieve a stable power output (Han et al., 2024).

The examples above highlight the necessity of accurately and completely modelling WEC subsystems to capture their characteristics properly. However, the WECs suitable for simulation within the DNV SESAM framework are limited to free-floating WECs with simple PTO and mechanical systems. This underscores the urgency of developing a new numerical framework which can mitigate the gap between the simulation requirements and the capabilities of the current DNV SESAM framework.

The FMI-based co-simulation framework can conveniently couple different tools and solvers without extra programming efforts. It has been successfully applied to model various engineering applications, such as hydraulic percussion units (Andersson et al., 2016, 2019, 2021), ships (Hatledal et al., 2020), hybrid vehicles (Yuan et al., 2020), hydraulic excavators (Gan et al., 2023), and cellular energy systems (Venzke et al., 2023). When applied to WEC system simulations, the FMI-based co-simulation framework can overcome the limitations of the DNV SESAM framework by coupling detailed PTO and mechanical system models developed separately in different software or custom-written programs and exported as FMUs. Each exported FMU acts as a black box, concealing the details of each subsystem model. The modelling and development of each subsystem can be distributed to teams with specific expertise as long as their models are encapsulated into FMUs. By properly defining and documenting the input and output pins, FMUs developed by different teams can easily integrate to form complex global simulations. This approach is particularly advantageous for multidisciplinary designs involving engineers from different fields. As the engineers no longer need to write communication programs to couple solvers and tools, they may focus solely on their areas of expertise. More importantly, the developed subsystem models can be reused and interchanged between different WEC concepts, which saves research costs and enables broader collaboration between WEC companies.

CHAPTER 3

Numerical models

This chapter introduces the numerical models developed for three WEC prototypes from three companies. Although all three can be categorised as point-absorber WECs that extract energy from heave motion, their working principles differ, entailing distinct modelling requirements and approaches. The two proposed numerical frameworks are chosen based on the characteristics of each WEC and their simulation goals. Through the numerical models of the three WEC prototypes, the features of the two numerical frameworks described in Section 2.7.3 can be better understood.

3.1 WaveEL 3.0 and WaveEL 4.0

Waves4Power AB is a wave energy company with a long history of over 50 years. Its WEC prototype, WaveEL, currently has two versions: WaveEL 3.0 and WaveEL 4.0. WaveEL 3.0 was successfully tested at full scale in 2017, and data were collected to guide the design of WaveEL 4.0 (Waves4Power, 2025a, 2025b). WaveEL is a point-absorber with a water piston inside its water tube attached to a hydraulic PTO system that converts heaving motion into electricity (Waves4Power, 2025c).

3.1.1 Hydrodynamic and mooring system models

Fig. 3.1 shows the WaveEL prototype in real installation and its mooring system configuration and hydrodynamic geometries. The synthetic mooring system consists of three legs spread out with angles of 120 degrees. Each mooring leg has two segments connected with a floater. The mooring lines are made of polyester whose

mechanical properties are adopted from Yang et al. (2020). As shown in Fig. 3.1b, Section 1 denotes the mooring section, which almost parallels the static water level. In contrast, Section 2 is the lower segment, which is connected with the anchor on the seabed. Section 1 is designed to remain under continuous tension to restrict horizontal motions, while its effects on the vertical motions are small due to its parallelism to the horizontal plane. The mooring length and pre-tension force are adjusted following the change in water depth and WEC version.

WaveEL 4.0 was developed based on WaveEL 3.0 with a longer acceleration water tube, as shown in Fig. 3.1c, designed to cope with different environmental conditions (ECs) and water depths. Besides the difference in the length of the acceleration water tube, the shapes of the upper bodies of WaveEL 3.0 and WaveEL 4.0 also differ slightly: the former has a circular upper cross-section, the latter a nonagonal one. Nonetheless, the upper part of both are roughly the same size, with diameters around 8 m.

In this thesis, the hydrodynamic and mooring systems are modelled under the two numerical frameworks so as to be integrated with PTO system models with different fidelity levels, which will be introduced in the following two subsections.

3.1.2 Simplified PTO system model

The actual working principle of a PTO system is far more complicated than that of a linear damper. The simplification is usually made for two main reasons. First, the behaviours of the PTO system are close to those of a linear damper, and the ultimate simulation goals do not require an in-depth analysis of what happens inside the PTO system. Second, even though the PTO system is sometimes more complex than a linear damper and involves non-linear features, this simplification is an inevitable compromise due to the limited tools and information available about the inner structures.

The PTO system of WaveEL WEC can be modelled as a linear damper with B_{PTO} equal to the radiated damping at the resonant frequency in the heaving direction without considering the mooring system (Yang et al., 2020). Accordingly, B_{PTO} for WaveEL 3.0 is taken as 40 kN/m and for WaveEL 4.0 as 50 kN/m. The power performance is calculated via Eq. (2.13).

The simplified PTO system can be easily modelled under the DNV SESAM framework and integrated with the hydrodynamic and mooring system models in the same framework. It can also be modelled in Simulink and connected with FMUs of other subsystems under the FMI-based co-simulation framework.

3.1.3 Detailed PTO system model

The working principles for WaveEL WEC are known. The FMI-based co-simulation enables the integration of a detailed PTO system model into other subsystem models.

(a) WaveEL 3.0 WEC.

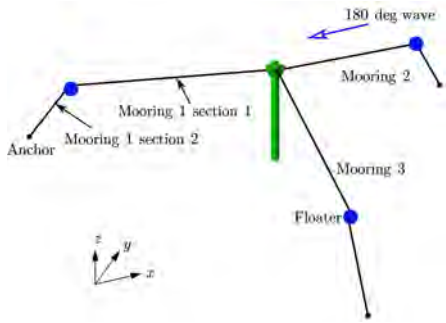

(b) WaveEL mooring system, adopted from **Paper D**.

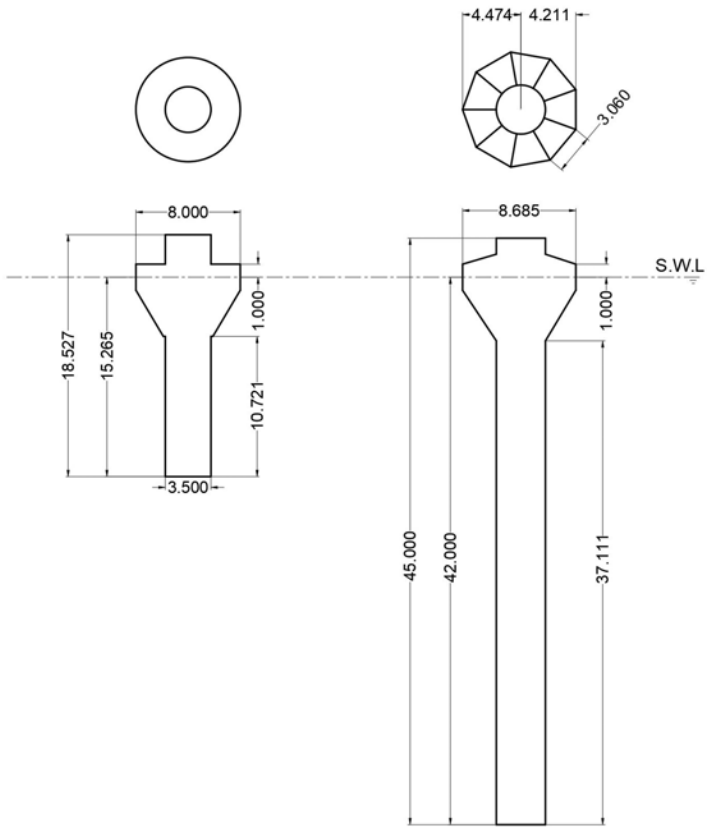

(c) Dimensions of WaveEL 3.0 (left) and WaveEL 4.0 (right), adopted from **Paper B**.

Figure 3.1: WaveEL WECs.

Therefore, the PTO system of WaveEL WEC is modelled in detail in this thesis to investigate the influence of the fidelity level of the PTO system model on the overall global simulation results.

The inner structures of the WaveEL PTO system and their terminologies are shown in Fig. 3.2. The piston rod of the hydraulic cylinder is fixed to the upper deck of the buoy hull. The hydraulic cylinder is sealed in a water-tight cassette containing the accumulator, hydraulic motor, and generator, which are not included in Fig. 3.2. The water piston is rigidly fixed to the cassette. When the buoy hull moves following the incoming waves, the water column inside the acceleration tube also oscillates, causing a relative motion between the water piston and the buoy hull that drives the hydraulic cylinder, from which hydraulic energy is converted into electricity by the hydraulic motor and generator. The bumpers are designed to limit excessive motions of the water piston and absorb rapid, intense impacts on the buoy hull, preventing damage under severe ECs.

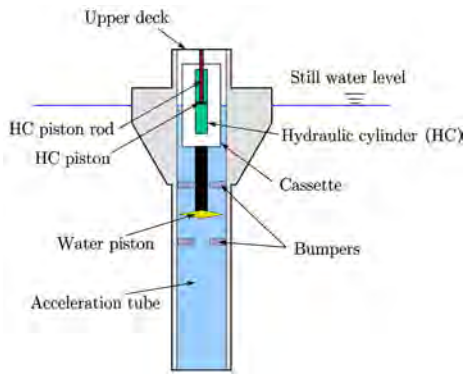

Figure 3.2: The inner structures of the WaveEL PTO system in **Paper E**.

The three main components of this detailed PTO system model are (1) the buoy hull, (2) the tube water, and (3) the water piston. The force naming convention is as follows: for instance, F_{31} represents a force exerted by component 3 (the water piston) on component 1 (the buoy hull) in the vertical direction. Specifically, the force from the bumper exerted on the water piston is F_{31b}. Therefore, the total vertical force exerted by the PTO system on the buoy hull is:

$$F_{PTO} = F_{31} + F_{31b} \tag{3.1}$$

Fig. 3.3 shows a diagram of the energy conversion path from the kinetic energy of wave elevations to electrical energy. For concision, the formulas involved in the detailed PTO system model are relegated to Section 3.2 of the appended **Paper E**. The detailed PTO system model is achieved in Simulink. It can be connected with FMUs of other subsystems to form a comprehensive global simulation.

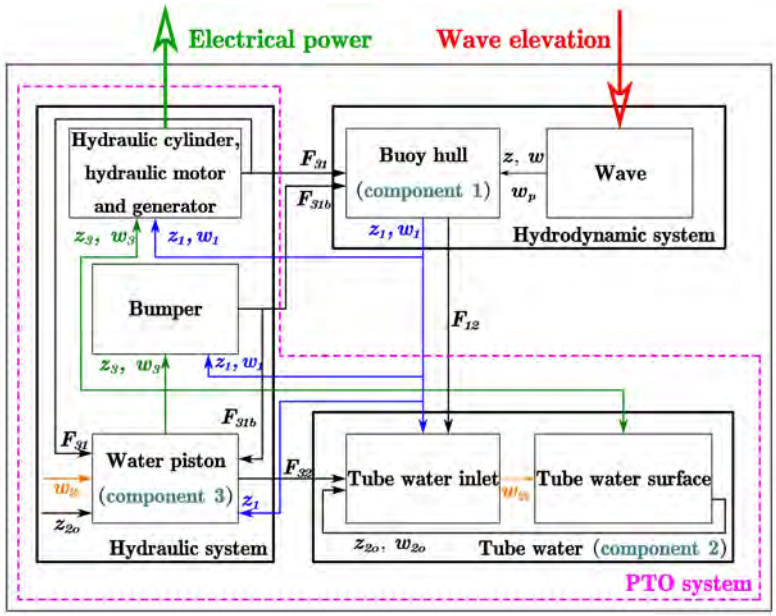

Figure 3.3: Diagram of the detailed WaveEL PTO system in **Paper E**.

3.2 CorPower

CorPower Ocean AB is one of the few wave energy companies to have reached a high technological readiness level (TRL) for floating WECs. Their WEC concept, CorPower, has been demonstrated and verified commercially from TRL 6 to TRL 7. TRL 7 indicates that the WEC prototype is close to its final design and functionality and has been tested in a similar environment to its intended operational conditions. The company is now actively demonstrating and type-certifying a pilot array with three WECs, which aims to take the technology from TRL 7 to TRL 8 (CorPower Ocean, 2025a, 2025b).

CorPower is a unique WEC prototype without mooring lines. Instead, the buoy is connected to a rigid rod connected to the seabed through a UMACK anchor, allowing free rotations. The main innovation of CorPower is shown in Fig. 3.4a. The WaveSpring provides negative spring stiffness, which results in amplified buoy motion and power performance. The cascade gearbox converts linear motions into rotations to drive the generators. The pre-tension cylinder provides downward force to compensate for extra buoyancy with reduced cost and low carbon footprint. The composite buoy is lightweight and low-cost. The UMACK anchor is a novel, efficient seabed anchoring system designed to reduce installation costs and improve stability for wave energy converters. It performs well regarding holding capacity, cost, carbon

footprint, and marine life friendliness (CorPower Ocean, 2025c).

The numerical model of CorPower WEC is shown in Fig. 3.4b. The model is built in the DNV SESAM framework with some simplifications. The rod connected to the seabed is modelled as a stiff mooring line, being modelled using mooring line tools but with high bending stiffness so that the buoy moves only along the mooring line's axial direction. The UMACK anchor is modelled using a supernode in Sima, which restricts any translations but allows free rotations. The modelling of other features of CorPower, such as WaveSpring, the pre-tension cylinder, and the PTO system model, are discussed in the following subsections.

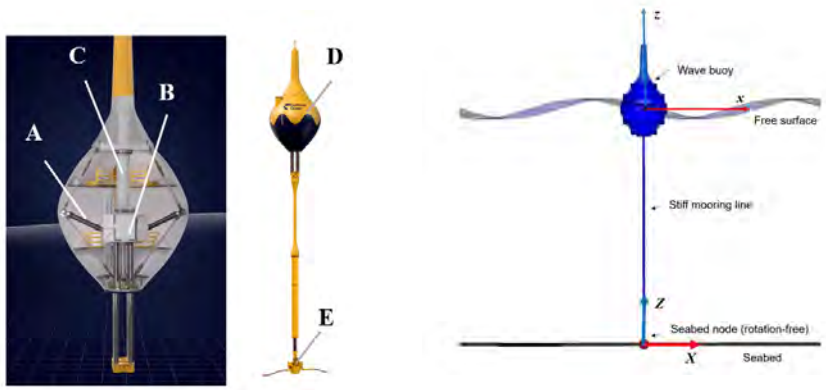

(a) CorPower WEC.

(b) CorPower numerical model, from **Paper C**.

Figure 3.4: CorPower structure and numerical model. The components in (a) are A: WaveSpring, B: Cascade gearbox, C: Pre-tension cylinder, D: Composite buoy, and E: UMACK anchor.

3.2.1 WaveSpring and pre-tension cylinder models

The negative stiffness the WaveSpring provides is -510kN/m. This value was chosen based on the experiments and tunings of the real WEC prototype by CorPower Ocean AB to make the numerical model closer to the real physical one. The pre-tension cylinder compensates for the extra buoyancy because the self-weight of the WEC is far less than the weight of the displaced water; the discrepancy between the self-weight and the buoyancy is 1.4×10^6 N. The WaveSpring and pre-tension cylinder features are modelled with the stiff mooring line shown in Fig. 3.4b.

3.2.2 Viscous drag force model

To better capture the forces exerted on the WEC, the drag elements are adapted to include the viscous drag force. As shown in Fig. 3.5, six cylindrical elements represent

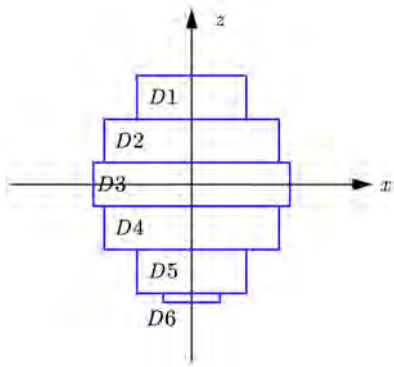

Figure 3.5: Viscous drag force model.

the varying diameters of the WEC. The radius and height of each drag element can be found in Table 2 of **Paper C**. The drag coefficients of heave, surge, and sway are 0.25, 0.5, and 0.5, respectively, values that CorPower Ocean AB provided based on their experiments and experience.

3.2.3 PTO system model

The real PTO system of CorPower WEC is complex, including the cascade gearbox and generators. However, detailed information about their structures and parameters is not available. As a compromise, the PTO system is modelled as a linear damper whose damping coefficient consists of two parts: useful damping and losing damping. The useful damping consists of various components that absorb wave energy and depends on the sea states. The losing damping, including machinery loss, is 25kNs/m. CorPower AB gave the values of the useful damping and the losing damping from their experiments. Exact values can be found in Table 3 of **Paper C**. The time-averaged hydrodynamic power performance can be calculated following Eq. (2.13), with the sum of the useful damping and the losing damping as B_{PTO}.

The end-stop bumpers within the PTO system are modelled as a nonlinear vertical force F_{es} whose primary function is to restrict heave motions from exceeding the pre-defined limit. The end-stop force is defined as:

$$F_{es} = -c\frac{z}{|z|}\left(|z| - z_{es}\right)^{n} \cdot H\left(|z| - z_{es}\right), \tag{3.2}$$

where z_{es} is the end-stop stroke and z is the WEC's vertical position, taking the static position as the origin. $H(\cdot)$ is the Heaviside function, and c and n are constants, here taken as $1 \times 10^{8}\mathrm{N/m}^{2}$ and 2. z_{es} is set to 3.4 m. These values are chosen based on the experiments and experience of CorPower Ocean AB.

3.3 NoviOcean

NoviOcean is a multiple-body WEC invented by the wave energy company Novige AB. A 1:2 scale physical model is shown in Fig. 3.6. Besides the buoys, the two main components are the water turbine and generator assembly inside the blue box and the hydraulic cylinder in the white dash box in Fig. 3.6.

As shown in Fig. 3.7, NoviOcean WEC has a piston rod fixed to the seabed anchor, allowing free rotation. Under incoming waves, the water tube and piston head will undergo relative motions that pressurise the water, which goes through the penstock to flush the water turbine on the top. The bottom-fixed piston rod couples the heave and the horizontal motions. This coupling must be captured by explicitly modelling the prismatic joint connecting the piston and the water tube.

The NoviOcean WEC is modelled under the FMI-based co-simulation framework. The global model can be divided into several subsystems whose modelling is discussed in detail in the following subsections.

3.3.1 Hydrodynamic and mooring system models

Fig. 3.8a shows the hydrodynamic and mooring system model of the NoviOcean WEC. The hydrodynamic system includes the buoy, the water tube, and the piston. The mooring system consists of four mooring lines, each comprising two sections. The same polyester material as for WaveEL WEC is used for this WEC. Similar to the mooring system of WaveEL, the two sections of each mooring leg of NoviOcean WEC are connected by a submerged floater. The hydrodynamic and mooring system parameters can be found in Table 2 of **Paper D**. It is worth noting that the turbine and generator assembly are not included in the hydrodynamic model because they are above the water level and, therefore, make no contribution to the hydrodynamic forces. The hydrodynamic and mooring systems are modelled in Ansys Aqwa and exported as an FMU.

Figure 3.6: NoviOcean WEC prototype model (scale 1:2) (Novige, 2023). The water turbine is in the blue box and the hydraulic cylinder in the dashed white box.

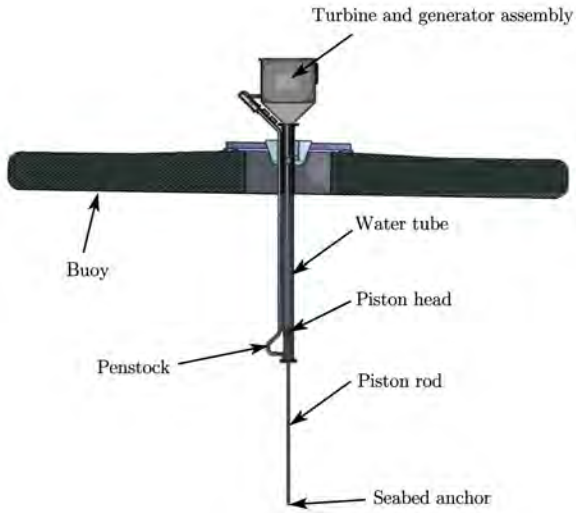

Figure 3.7: The inner structures, from **Paper D**.

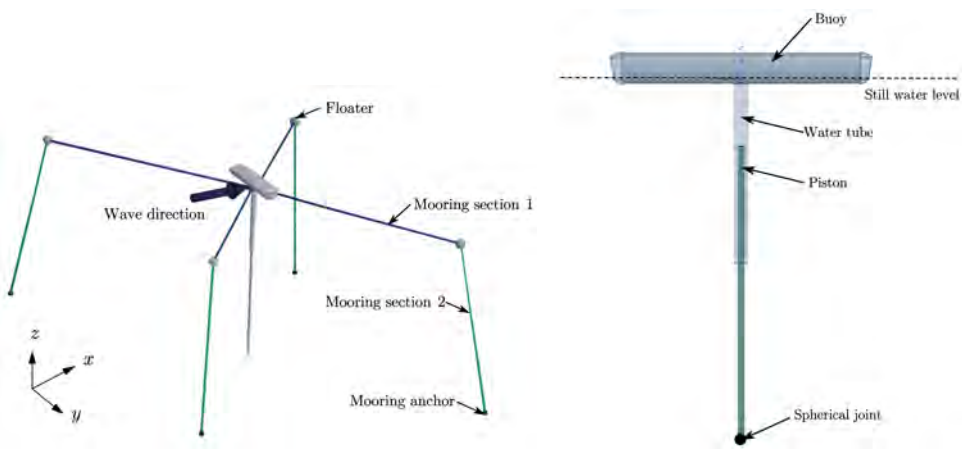

(a) **(b)**

Figure 3.8: NoviOcean numerical models, from **Paper D**. (a) The hydrodynamic and mooring system model, and (b) the mechanical system model.

3.3.2 Mechanical system model

The mechanical system model is shown in Fig. 3.8b. In the NoviOcean WEC, the mechanical system consists of joint connections. The first is a prismatic joint between the piston rod and the water tube, while the second is a spherical joint between the piston and the seabed. The two joints are modelled in Ansys Rigid Dynamics and exported as an FMU.

3.3.3 PTO system model

The real PTO system of NoviOcean is a complex subsystem comprising hardware components such as the water turbine and generator and software like control algorithms. However, very little detailed information on these components was available during the thesis. Therefore, the PTO system model of NoviOcean is once again simplified as a linear damper whose damping coefficient, B_{PTO}, is equal to the radiation damping at different wave periods. The choice of B_{PTO} is inspired by the optimal PTO control method in the frequency domain, as referenced in Alves (2016).

The optimal PTO control requires twofold conditions. First, the PTO reactance, defined as K_{PTO}/ω, where K_{PTO} is the PTO stiffness and ω the wave angular frequency, should cancel out the inherent reactance, which includes the reactance caused by the mooring stiffness and hydrostatic stiffness. Second, the PTO damping B_{PTO} should equal the radiation damping. However, in the linear damper PTO system model, only the second condition is satisfied, as the inherent reactance is difficult to determine.

The radiation damping of the NoviOcean WEC at different wave periods is shown in Fig. 3.9. The calculated radiation damping exists only for discontinuous wave period selection in BEM solvers. Therefore, an interpolation method is applied to obtain a fitted radiation damping curve. The PTO damping is then determined from the fitted curve for different wave periods.

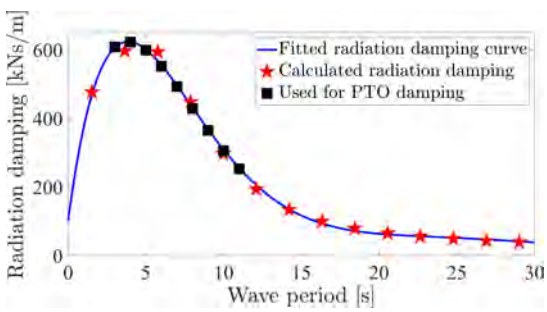

Figure 3.9: PTO damping coefficients for NoviOcean WEC, from **Paper D**.

3.4 Numerical models for wave parks

The wave park layouts in this Section are promising designs proposed by the companies for future real installations.

3.4.1 WaveEL wave parks

Three wave park layouts have been developed for WaveEL WECs, as illustrated in Fig. 3.10. Their key parameters are listed in Table 3.1. Further details of the wave parks can be found in the corresponding papers listed in the last column.

StarBuoy is a 10-WEC wave park, which was found to be the best candidate for the sea conditions in the Runde test site in Norway from the perspectives of LCoE, risk, and mooring fatigue analyses (Ringsberg et al., 2020a). Hex1 and Hex2 evolved from StarBuoy, with the WECs reduced from 10 to 6. The symmetric layouts enable them to cope with changing incident wave direction under real sea states.

The three wave parks have similar parameters, as listed in Table 3.1. R is the radius of the footprint area of the whole wave park, while r is the radius of a single WEC unit within the park. The distance between units is defined as the separation between two neighbouring units. From StarBuoy to Hex1-120, R keeps a similar value to maintain a similar footprint area. From Hex1-120 to Hex1-80, the distance between each WEC is further reduced to save the length of mooring lines and reduce the footprint area. Hex2 is developed from Hex1-120 by keeping a similar r but not sharing the centre anchor.

The WEC units installed in the three wave parks can be WaveEL 3.0 or WaveEL 4.0. To meet various simulation goals, the PTO system model of each WEC unit in a wave park can be a simplified linear damper or a detailed PTO model. The numerical model of wave park Hex1-80 equipped with detailed PTO system models in **Paper E** under the FMI-based co-simulation framework is shown in Fig. 3.11.

Table 3.1: Parameters of the WaveEL wave parks and their appearance in papers.

Wave park	WEC number	Distance [m]	R [m]	r [m]	Paper
StarBuoy	10	52	200	100	**A**
Hex1-80	6	80	139	80	**A, B, E**
Hex1-100	6	120	173	100	**B**
Hex1-120	6	120	208	120	**A, B**
Hex2	6	260	390	130	**A**

3.4.2 CorPower wave parks

The two wave park layouts for the CorPower WEC are illustrated in Fig. 3.12. Both contain 16 WECs, with the units at a distance d in both the horizontal and vertical

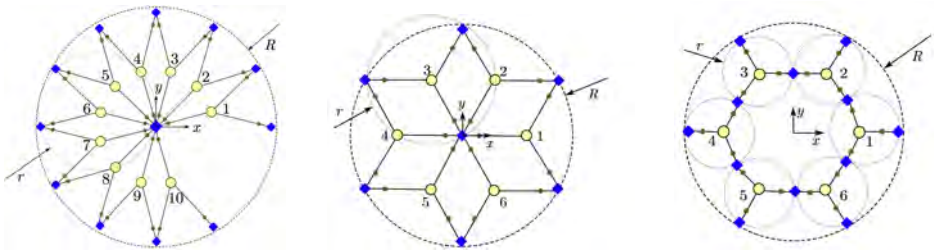

(a) StarBuoy. **(b)** Hex1. **(c)** Hex2.

Figure 3.10: WaveEL wave parks, from **Paper A**. The yellow circles represent the WEC units, the green circles represent the floaters, the blue squares represent the anchors, and the black lines represent the mooring lines. The wave direction is defined as the angle between the wave incoming direction and the positive x-axis.

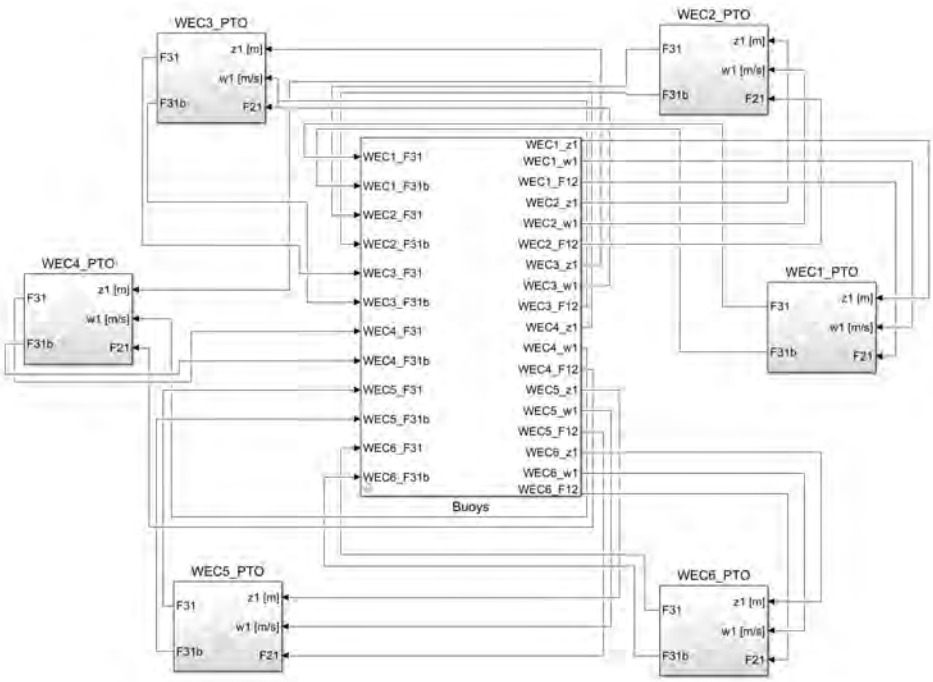

Figure 3.11: Simulink model for Hex1-80 wave park with detailed PTO systems in each WEC, from **Paper E**.

directions. The 4×4 layout has four WECs in each row and column, while the 8×2 layout has eight WECs per row spread across two rows. The 8×2 layout is broader, with more columns than the 4×4 layout. These two wave park layouts were designed to maintain the same total footprint area while varying the number of rows and WECs per row to examine their impact on the power performance of the wave park. Additionally, the square and rectangular shapes facilitate easier installation of multiple WECs and the laying of power cables.

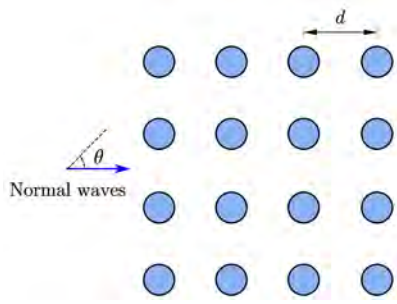

(a) 4x4.

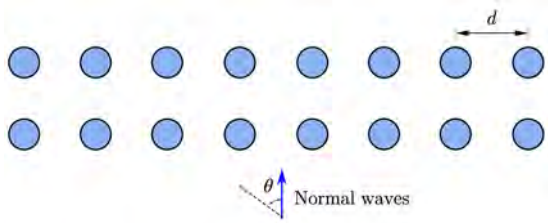

(b) 8x2.

Figure 3.12: CorPower wave parks, from **Paper C**.

3.4.3 NoviOcean wave park

The NoviOcean wave park consists of 18 WECs, as shown in Fig. 3.13. The wave park is designed with a staggered pattern to reduce the shadowing effect of the frontline WECs. The NoviOcean wave park model is built under the FMI-based co-simulation framework. The separation distance between the WECs along the x- and y-axes is 100 m, selected to ensure that the wave park remains compact.

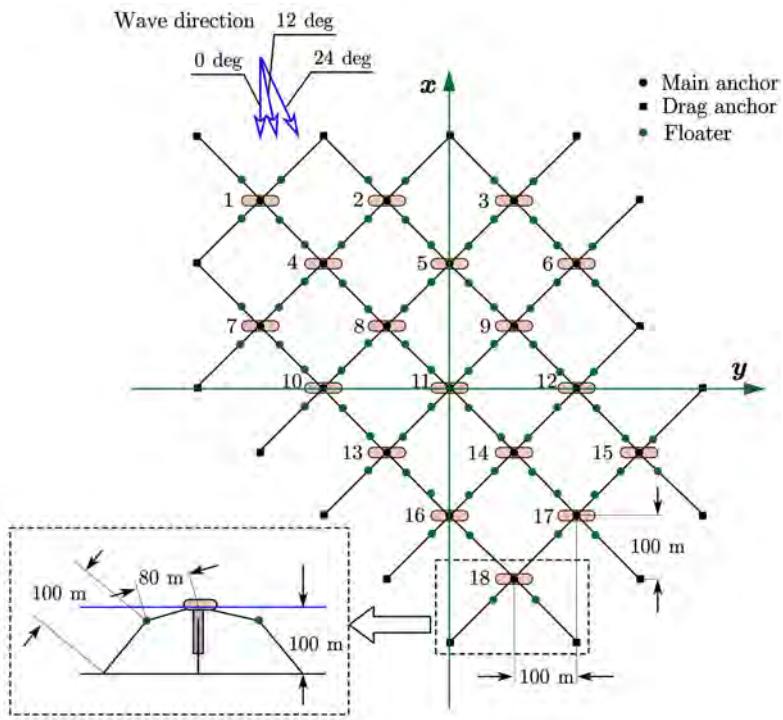

Figure 3.13: NoviOcean wave park, from **Paper D**.

CHAPTER 4

Verification and validation

This chapter intends to verify and validate the proposed two numerical frameworks rather than numerical models of specific WECs for several reasons. Throughout the period of the project, WEC technology rapidly evolved, and due to the limited funding, it was not feasible to perform experimental validation for specific WECs. Accordingly, code-to-code verification efforts have been directed towards ensuring the correctness and internal consistency of the numerical frameworks themselves. Validation is constrained by the limited availability of experimental data for specific WECs, but an effort has been made to enhance the credibility of the numerical frameworks through comparisons with benchmark cases. Additionally, a partial validation of one WEC prototype has been performed using a small set of historical real measurement data.

Through verification and validation, the general confidence in the numerical frameworks for simulating coupled systems increases, which supports their potential application to other renewable energy devices, such as offshore wind turbines.

4.1 Benchmark study – experimental heave decay test

The benchmark study carried out in the Ocean and Coastal Engineering Laboratory wave basin at Aalborg University (Kramer et al., 2021) was chosen to verify and validate the FMI-based co-simulation framework. As illustrated in Fig. 4.1, an aluminium sphere with a diameter D of 300 mm was dropped from three heights, $0.1D$, $0.3D$, and $0.5D$, representing linear, moderately nonlinear, and highly non-

linear cases. This benchmark study provides a rigorous experimental database for numerical model validations. Therefore, a co-simulation model adopting the same physical parameters as in the experiments was built to demonstrate the capability of each FMU to perform subsystem simulations and of the FMI-based co-simulation to handle multi-solver communications.

Besides experimental data, the benchmark study provides several datasets from numerical simulations using various numerical models. The linear potential flow model 2 (LPF2) is one of these, which uses nonlinear draft-dependent hydrostatics and linear hydrodynamics coefficients. It is also included in the comparison because it has the same level of numerical complexity in representing the hydrostatic and hydrodynamic forces as the co-simulation model. The degree of agreement between the results for LPF2 and the co-simulation model demonstrates the closeness of the capability of the FMI-based co-simulation and other numerical methods. It can thus help verify the ability of the FMI-based co-simulation framework to provide results consistent with those of other numerical methods.

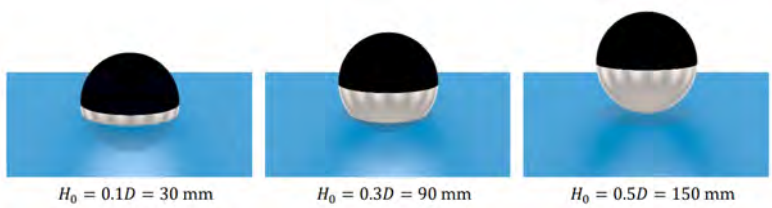

Figure 4.1: Tested initial submergences and drop heights from Kramer et al. (2021).

Qualitatively, Fig. 4.2 compares the co-simulation results and the benchmark datasets. For a more effective comparison, the heave decay time series is normalised by the drop height, while time is scaled using the damped natural period in heave, which is 0.76 s, as stated in Kramer et al. (2021). It is observed that for the dropping heights of $0.1D$ and $0.3D$, the difference between the results is almost negligible. A noticeable difference is observed for the dropping height of $0.5D$, but this is not due to the shortcomings of the co-simulation method, but rather to the limitations of linear potential theory in handling nonlinearity arising from large motions, as the results for LPF2 also show similar discrepancies from the experimental data.

Quantitatively, the root mean square errors (RMSEs) between each pair of the three time series are compared in Fig. 4.3, and the Pearson correlation coefficient ρ between the three time series are listed in Table 4.1. The nonlinear case with a drop height of $0.5D$ exhibits the highest RMSE among the three scenarios. However, even in this case, the RMSE of 0.063 remains relatively small compared to the initial normalised drop height of 1. Meanwhile, the RMSEs between LPF2 and the co-simulation results do not exceed 0.015 in any of the cases, demonstrating strong agreement. Moreover, the closer ρ is to 1, the stronger the linear correlation between

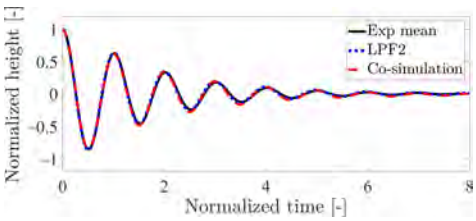

(a) Dropping height of $0.1D$.

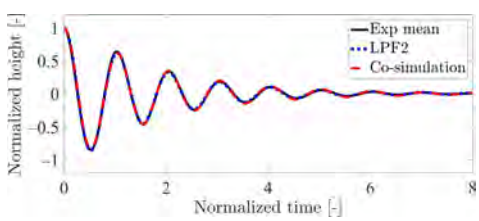

(b) Dropping height of $0.3D$.

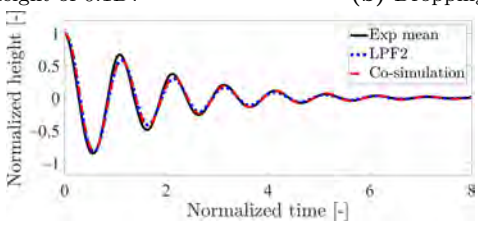

(c) Dropping height of $0.5D$.

Figure 4.2: Benchmark study – dropping sphere heave decay test, from **Paper D**.

the two time series. In all cases, the correlation coefficient for each pair of the three time series exceeds 0.98, indicating a strong linear relationship.

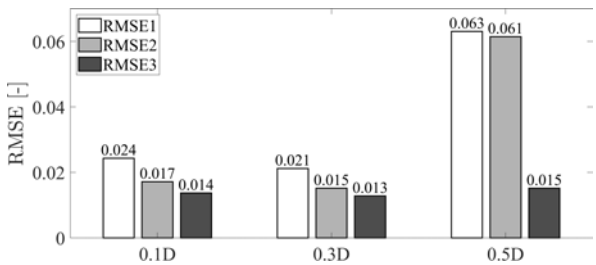

Figure 4.3: RMSE values of the time series, from **Paper D**. RMSE1 is the RMSE between the experimental and co-simulation results, RMSE2 is the RMSE between the experimental and LPF2 results, and RMSE3 is the RMSE between the LPF2 and co-simulation results.

The RMSEs and correlation coefficients demonstrate that the co-simulation results align well with the experimental and LPF2 results. The agreement between the LPF2 and co-simulation results verifies each FMU's capability to perform its respective subsystem simulation and the effectiveness of Simulink's co-simulation algorithm in managing multi-solver communications. The agreement with experimental data provides a further level of validation, indicating that the framework can accurately capture key physical behaviours.

Table 4.1: Correlation coefficients. ρ_1 is the correlation coefficient between the experimental and co-simulation results, ρ_2 is the correlation coefficient between the experimental and LPF2 results, and ρ_3 is the correlation coefficient between the LPF2 and co-simulation results.

	ρ_1	ρ_2	ρ_3
$0.1D$	0.9981	0.9996	0.9996
$0.3D$	0.9981	0.9995	0.9993
$0.5D$	0.9895	0.9993	0.9899

4.2 Code-to-code verification

The two numerical frameworks, DNV SESAM and FMI-based co-simulation, are cross-verified by comparing the numerical results for the WEC motions, mooring forces, and power performance of a WaveEL 4.0 WEC and a wave park, both modelled within these frameworks.

4.2.1 Single WaveEL 4.0 WEC

The numerical models of the single WaveEL 4.0 WEC under the two numerical frameworks keep the values of all the physical parameters, such as the dimensions and the linear damping coefficient, the same for better comparison. Information on the geometrical dimensions and fundamental properties of WaveEL 4.0 is available in **Paper B**. The tested case is under a regular wave condition with an amplitude of 1 m and a wave period of 6.5 s.

WEC motions and mooring forces

Figs. 4.4 and 4.5 illustrate a comparison of the WEC motions and mooring forces obtained from the co-simulation and DNV SESAM model over a 400 s duration. Since Moorings 1 and 3 are symmetrically positioned for the wave direction, their tension values are identical. Therefore, only the Mooring 2 and 3 results are presented in Fig. 4.5. Table 4.2 provides the RMSEs and correlation coefficients between the results from the two numerical frameworks to assess quantitatively the discrepancies between the two models. The correlation values are close to 1, demonstrating a strong agreement between the datasets.

For the heave motion, which plays an important role in predicting the power output of this heaving point absorber, the RMSE amounts to approximately 5% of the heave amplitude (around 2 m), indicating a relatively minor deviation. In contrast, the surge motion exhibits slightly more significant differences, with an RMSE around 14% of its amplitude. This discrepancy is primarily due to an upward shift in the co-simulation results compared to the DNV SESAM model. Despite this shift, the

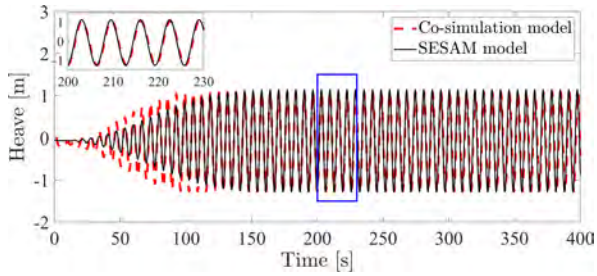

(a) Heave motion.

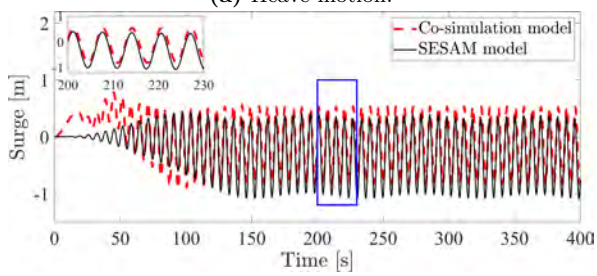

(b) Surge motion.

Figure 4.4: Heave and surge motions of WaveEL 4.0, from **Paper D**. The time series with the blue-line box is magnified in the upper left corner of each figure.

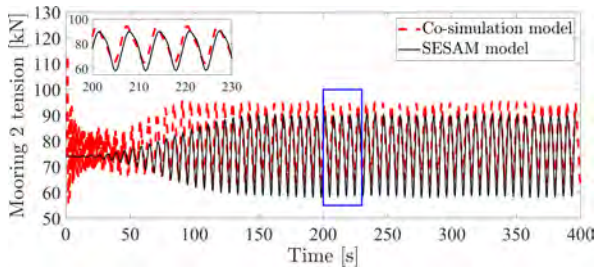

(a) Mooring 2.

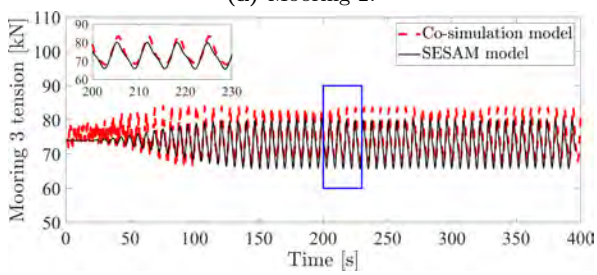

(b) Mooring 3.

Figure 4.5: Mooring forces of WaveEL 4.0, from **Paper D**. The time series with the blue line box is magnified in the upper left corner of each figure.

Table 4.2: RMSMs and correlation coefficients of the results of the co-simulation and SESAM models. The analysed time series begin from 150 seconds to avoid the unstable starting phase.

	RMSE	ρ
Heave	0.1177 m	0.9917
Surge	0.2123 m	0.9893
Mooring 2	4.2014 kN	0.9773
Mooring 3	2.6390 kN	0.9719

amplitudes of the surge motion remain nearly identical. Given that heave is more significant than surge in power performance estimation, the variation in surge motion is considered to fall within an acceptable range.

The displacement shift in the co-simulation results also leads to a shift in mooring forces, as depicted in Fig. 4.5. The RMSE values for Mooring 2 and Mooring 3 amount to approximately 14% and 15% of their respective amplitudes. However, unlike heave and surge, which oscillate around zero, the mooring tensions centre around their pretension force of roughly 74 kN. Compared to these mean values, the RMSEs of mooring forces correspond to about 6% and 4%, suggesting minor discrepancies.

Overall, the evaluation of RMSEs and correlation coefficients confirms that the co-simulation approach can model WEC systems with coupled subsystems and produce motion and mooring force predictions closely aligned with those from the DNV SESAM framework.

Power performance

The power performance under three regular wave conditions listed in Table 4.3 is compared in Fig. 4.6 for a single WaveEL WEC modelled under the two numerical frameworks. The results show good agreement for EC1 and EC2 in cases of relatively low wave heights. For EC3, the case with the highest wave height, the deviation between the two models remains below 8%. This suggests that both approaches produce comparable results when simulating a single WEC with a linear-damper PTO system under regular ECs. The observed differences may stem from minor mooring configuration and water depth variations.

Table 4.3: ECs for simulations.

EC	Wave amplitude A [m]	Wave period T [s]	Wavelength [m]
EC1	0.25	4.5	31.6
EC2	0.75	5.5	47.2
EC3	1.75	7.5	87.8

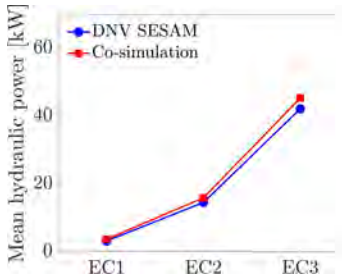

Figure 4.6: Single-WEC performance comparison with a linear-damper PTO system model. The results of DNV SESAM come from **Paper A**.

4.2.2 Wave park

Figure 4.7 compares the power performance predictions for a six-WEC array. Similar to the single-WEC analysis in Section 4.2.1, the wave park model employs a linear damper to represent the PTO system. The co-simulation results exhibit interaction patterns comparable to those obtained from DNV SESAM, demonstrating that the co-simulation approach effectively captures the interaction effects among WECs within a wave park.

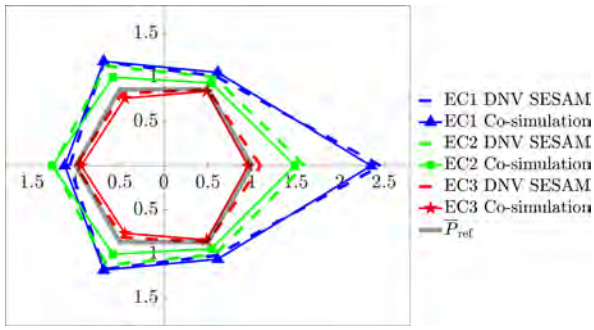

Figure 4.7: Wave park performance comparison with a linear-damper PTO system model from **Paper E**. The results of DNV SESAM come from Shao et al. (2024).

4.3 Validation of the WaveEL model against limited real test site data

WaveEL is one of the studied WECs whose historical real measurement data are available. This WEC operated at full capacity throughout the measurement campaign from June to November 2017 (Ringsberg et al., 2020b). The available measurement

data under the three ECs listed in Table 4.4 are used to perform a limited validation of the numerical model of a single WaveEL 3.0 WEC, developed within the DNV SESAM framework, as presented in **Paper B**. The limited amount of real measurement data makes it impossible to comprehensively validate the numerical model built under the DNV SESAM framework. However, the qualitative comparison results are included in this section to enhance the credibility of the DNV SESAM framework for WEC simulations.

Table 4.4: Sea state conditions (long-crested waves), from Ringsberg et al. (2020b).

Date and time	H_s [m]	T_p [s]	Wave direction θ [deg]
2017-06-16 10:00-13:00	0.95	10.00	30
2017-06-18 08:00-11:00	1.40	6.75	30
2017-06-19 15:00-18:00	1.75	7.50	30

The WEC prototype used in the real measurement was WaveEL 3.0. However, the results for WaveEL 4.0 are also compared against the real measurement data to evaluate the performance of both versions. Since the differences between the two versions are deemed small, it is assumed that if the results for WaveEL 4.0 align closely with the real measurement data of WaveEL 3.0, confidence in the numerical model of WaveEL 4.0 will be enhanced. The axial forces in the moorings were first adjusted to align with the real measured data to ensure that the real measurements and simulations had similar mooring forces, leaving the WEC motion as the only variable remaining for comparison. As shown in Fig. 4.8, the time-averaged axial forces within the leading and rear mooring lines generally show good agreement with the measured data, with an error of less than 10%.

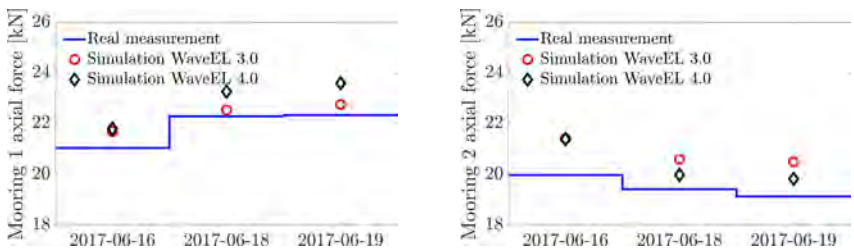

(a) Axial force in the upper section of Mooring 1.

(b) Axial force in the upper section of Mooring 2.

Figure 4.8: Time-averaged mooring forces validations, from **Paper B**. Mooring 1 is the leading mooring, which aligns with the incoming waves. Moorings 2 and 3 are the rear moorings, symmetric relative to the incoming wave direction.

The WEC motions are compared in Fig. 4.9. In general, as shown in Fig. 4.9a and 4.9b, the WEC position points recorded during the experiments are distributed

within the regions that overlap with the envelopes obtained from the simulations. However, for the other validation cases shown in Fig. 4.9c - 4.9f, the simulated horizontal motions of the WEC are inclined to the incoming wave direction, while the real measurements are more scattered than the numerical results. The reason is that the wave directions constantly changed during the real test, while the estimated sea states for simulations only considered the dominant wave directions.

It may be observed that the range of motion of WaveEL 4.0 tends to be larger than that of WaveEL 3.0. The vertical range of motion of the WaveEL 3.0 model agrees well with the experiment, which qualitatively validates the numerical model.

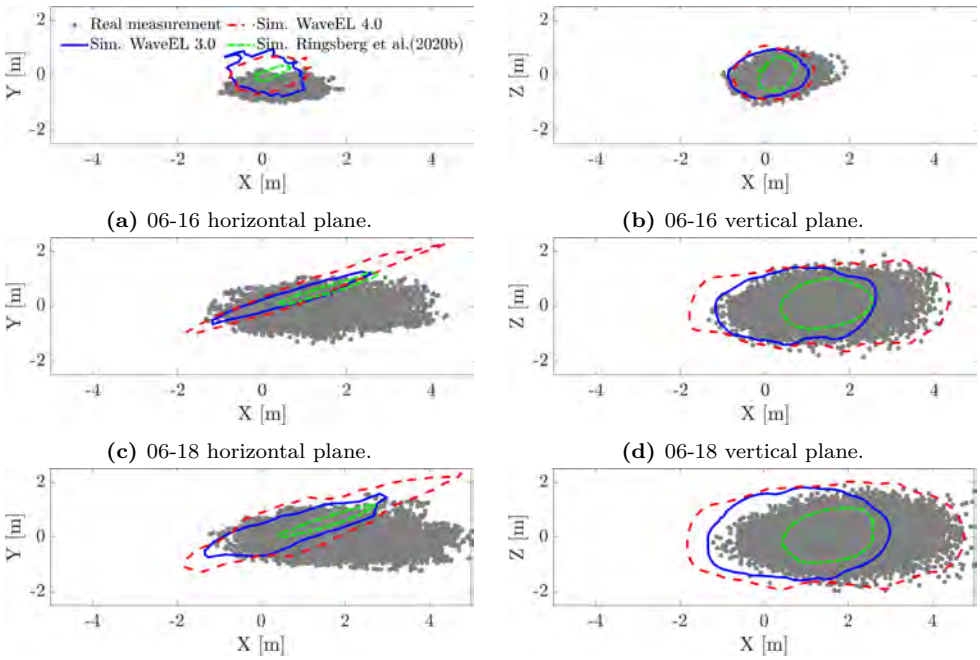

(a) 06-16 horizontal plane.

(b) 06-16 vertical plane.

(c) 06-18 horizontal plane.

(d) 06-18 vertical plane.

(e) 06-19 horizontal plane.

(f) 06-19 vertical plane.

Figure 4.9: WEC motion range comparison, from **Paper B**.

CHAPTER 5

Summary of papers

This section summarises the representative results and main findings of each paper to show the capability of the numerical frameworks. Fig. 5.1 shows the contributions of each paper to the thesis structure. **Papers A–C** contain simulations carried out under the DNV SESAM framework, while the models in **Papers D–E** are based on the FMI-based co-simulation framework.

Paper A investigates only the power performance of single WECs and wave parks with different layouts. **Paper B** introduces mooring fatigue damage as another factor when evaluating wave park designs. **Paper C** applies the same DNV SESAM framework to CorPower, a bottom-fixed WEC prototype without mooring lines, and estimates the power performance of a 16-WEC wave park. Due to the limitations of the DNV SESAM framework, the PTO and mechanical system models are simplified in **Papers A–C**.

Papers D–E adopt the FMI-based co-simulation framework to better capture the effects of the PTO and mechanical systems on power performance and mooring fatigue damage. NoviOcean WEC is chosen as a study object in co-simulations in **Paper D** because of its unique working principle. An 18-WEC wave park design is also analysed in **Paper D** to demonstrate the capability of the FMI-based co-simulation framework in simulating wave parks with many WECs. Finally, **Paper E** completes the thesis by integrating detailed PTO systems into single WECs and wave parks. **Paper E** emphasises the importance of modelling the PTO system in detail when the nonlinear components, such as bumpers, come into effect.

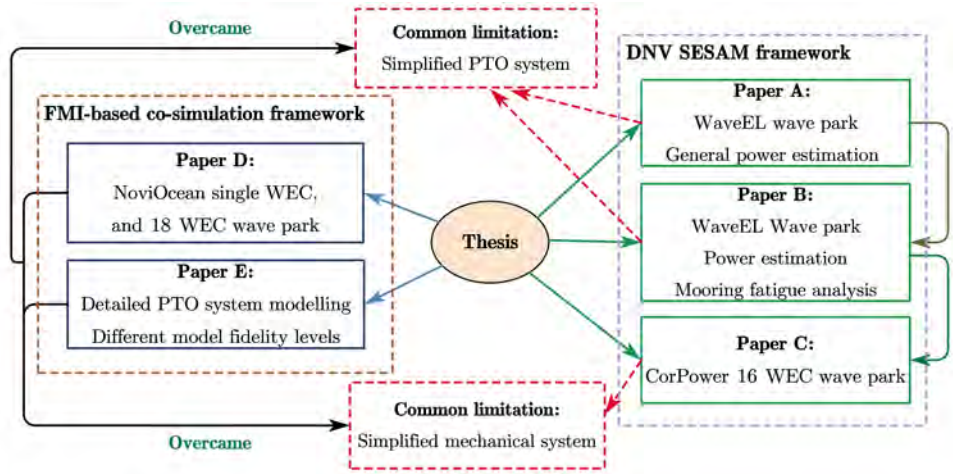

Figure 5.1: Thesis structure and connections between papers.

5.1 Summary of Paper A

"Performance analysis of two generations of heaving point absorber WECs in farms of hexagon-shaped array layouts"

The purpose of **Paper A** is to compare the power performance of two versions of WaveEL WEC, WaveEL 3.0 and 4.0, for a single unit and wave parks. The numerical models were built under the DNV SESAM framework. The analysed wave parks are described in Section 3.4.1, and three representative ECs with regular waves listed in Table 4.3 were simulated for the wave parks.

A frequency domain response analysis was carried out for WaveEL 3.0 and 4.0. As shown in Fig. 5.2a, the resonance periods for the two versions of WEC are different, with WaveEL 3.0 at 4 s and WaveEL 4.0 at 5 s. This difference results from the geometrical differences in the WEC designs, as WaveEL 4.0 has a longer water tube than WaveEL 3.0.

The power performance of single WECs under different ECs is compared in Fig. 5.2b. In general, WaveEL 4.0 outperforms WaveEL 3.0 under all ECs. There are two reasons for this. First, the PTO system model used is the linear damper model described in Section 3.1.2, where the damping coefficient for WaveEL 4.0 (50 kN/m) is 25% higher than that for WaveEL 3.0 (40 kN/m). Therefore, according to Eq. (2.13), the increased PTO damping coefficient from WaveEL 3.0 to WaveEL 4.0 accounts for 25% of the power performance increase if the heave motions are the same. However, under EC1, the increase in power performance of WaveEL 4.0 compared to WaveEL 3.0 is less than 25%. In contrast, under EC2 and EC3, the increase exceeds 55%. This is because the geometrical changes lead to different heave amplitude response

patterns under regular waves, as shown in Fig. 5.2a.

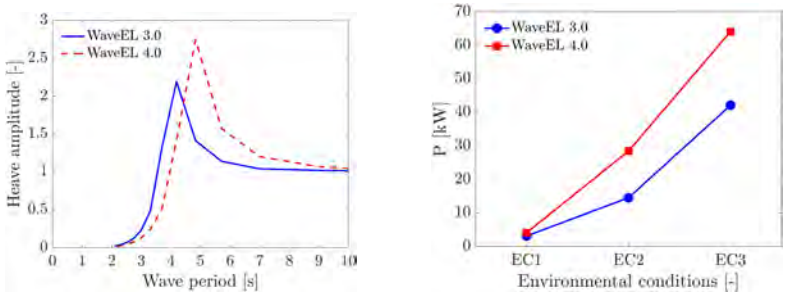

(a) Heave response in the frequency domain.

(b) Power performance under regular waves.

Figure 5.2: Single WaveEL WEC performance.

The power performance of each WEC within a wave park under various ECs and wave directions was analysed and compared. Fig. 5.3 shows the normalised power performance of wave park Hex1-80 under three ECs with the wave direction of 180 degrees. The normalisation was done by dividing the power performance of each WEC by that of a single WEC under the same EC. Therefore, a larger-than-one normalised power performance indicates positive interaction effects. Under EC1 and EC2, the power performances of most of the WECs are larger than one, indicating positive interaction effects, while under EC3, the normalised power performances of the wave parks, whether using WaveEL 3.0 or WaveEL 4.0, are close to 1, reflecting negligible interaction effects on power performance. For both WEC versions, the leading WEC encounters the waves first and has the largest power performance. Comparing wave parks equipped with different WEC versions, the WaveEL 4.0 wave park is more sensitive to changes in EC.

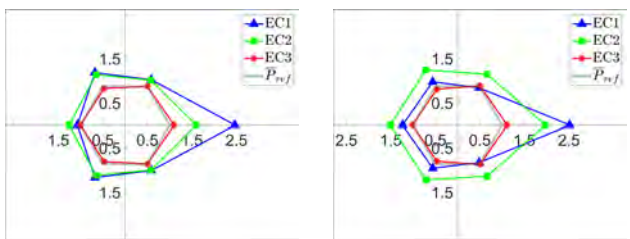

(a) WaveEL 3.0.

(b) WaveEL 4.0.

Figure 5.3: Wave park Hex1-80 power performance normalised by single-WEC power performance. The waves come from 180 degrees, from right to left.

Fig. 5.4 shows the influence of the wave direction on the power performance of each WEC within a Hex1-80 wave park under EC2. The wave directions were

changed from 150 to 180 degrees at 10-degree intervals. The results indicate that under all the simulated wave directions, the interaction effects are constructive, as the WECs within the wave park exhibit a normalised power performance larger than one. However, the relative power performance of each WEC within the wave park varies with changes in the incoming wave direction. For example, the WEC positioned furthest upstream generates the highest power with 180-degree waves, while the two WECs located furthest downstream attain maximum power with 150-degree waves.

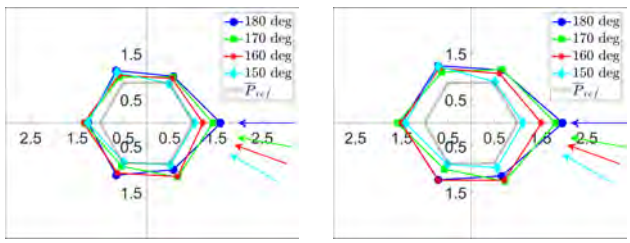

(a) WaveEL 3.0. **(b)** WaveEL 4.0.

Figure 5.4: Wave park Hex1-80 normalised power performance under EC2 with different wave directions.

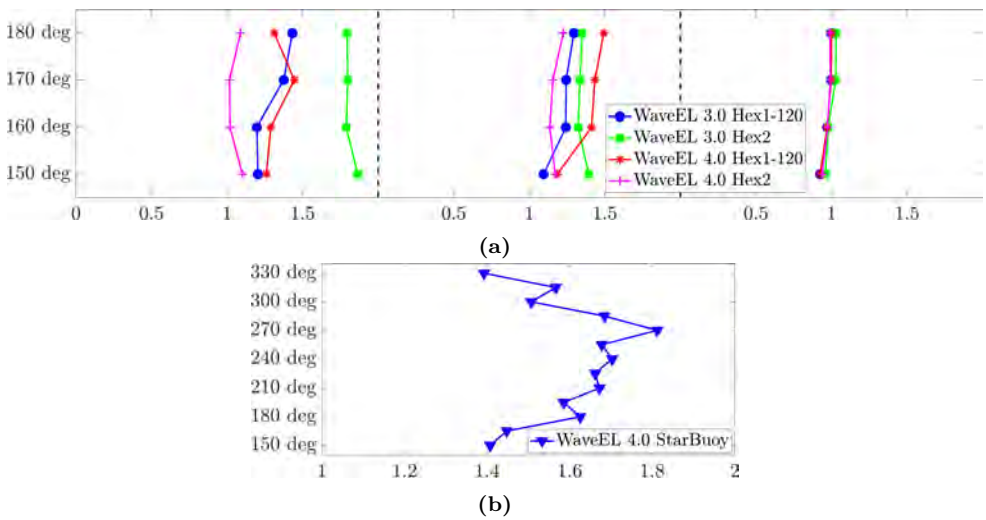

Figure 5.5: (a) Normalised total power performance for hexagonal wave parks. From left to right, divided by dashed black lines, EC1 to EC3. (b) Normalised total power performance for StarBuoy wave park equipped with WaveEL 4.0 under EC2.

The total power performance of a wave park was analysed and compared for varying layouts, wave conditions, and wave directions. In Fig. 5.5a, the total normalised

power performances of two wave parks, Hex1-120 and Hex2, are compared. Overall, deploying multiple WECs in a wave park does not exert a negative influence on the total power performance, as the normalised total power performance is almost always larger than one under all the simulated situations. Under EC1, the Hex2 wave park with WaveEL 3.0 exhibits the highest normalised total power performance, and its performance is not sensitive to wave direction changes. However, this is not the case under EC2, where the Hex1-120 wave park with WaveEL 4.0 has the highest normalised total power performance with most wave directions. The StarBuoy wave park with WaveEL 4.0 was also simulated under EC2, as shown in Fig. 5.5b. It demonstrates an even higher normalised total power performance than the Hex1-120 wave park, with values exceeding 1.4 for waves from 150 degrees to 330 degrees. Under EC3, the interaction effects on power absorption are minimal or slightly negative for all the wave parks.

5.2 Summary of Paper B

"A comparison of two wave energy converters' power performance and mooring fatigue characteristics – One WEC vs many WECs in a wave park with interaction effects"

The focus of **Paper B** is broadened from the pure power performance analysis of wave parks in **Paper A** to a combined study of power performance and mooring fatigue damage. Three cases were simulated with the ECs defined in Table 5.1. These cases represent irregular waves that had a high probability of occurrence at the Runde test site in 2017. All cases listed in Table 5.1 are irregular waves modelled using the JONSWAP wave spectrum with a peak enhancement factor of 2.4.

Table 5.1: Definitions of the three sets of ECs and the probabilities of their occurrence at the Runde test site.

IR-EC	H_s [m]	T_p [s]	Probability of occurrence [%]
IR-EC1	0.5	4.5	6.84
IR-EC2	1.5	5.5	10.14
IR-EC3	3.5	7.5	5.63

The accumulated mooring fatigue damage was thoroughly investigated in **Paper B**. The simulations were conducted for a physical time of 1 hour, and the mooring force responses over this period were used for fatigue analysis. Fig. 5.6 shows the accumulated mooring fatigue damage of all the mooring lines in the Hex1-80 wave park, assuming that the 1-hour simulation is repeated continuously for one year under IR-EC2. The largest fatigue damage for each WEC unit was identified and connected

by dashed lines. The results indicate that with varying wave directions, the mooring lines of the leading WECs usually experience the most significant fatigue damage.

Furthermore, the weakest link is defined as the mooring line in the wave park that suffers the greatest accumulated fatigue damage. The mooring system is considered to have failed if the accumulated fatigue damage of the weakest link exceeds 1. Fig. 5.7 presents the accumulated fatigue damage of the weakest link of the Hex1-80 wave park, comparing two versions of WEC under varying ECs. Results show that under IR-EC2 and IR-EC3, the wave park equipped with WaveEL 4.0 tends to experience larger fatigue damage than WaveEL 3.0. However, even in the worst-case scenario, which occurs in the WaveEL 4.0 wave park under IR-EC3, the estimated mooring fatigue life exceeds 100 years, assuming that the simulated ECs persist for an extended period.

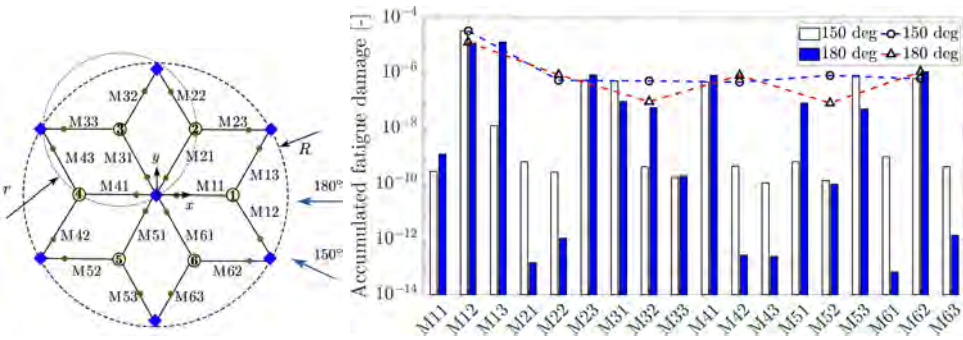

(a) **(b)**

Figure 5.6: (a) Mooring line numbering of Hex1 wave park. (b) The accumulated fatigue damage of each mooring line in Hex1-80 wave park with WaveEL 4.0 with incoming wave directions of 150 and 180 degrees under IR-EC2. The lines show the accumulated fatigue damage of each WEC unit.

Simulations were conducted for wave parks with three different inter-unit distances for the Hex1 wave park. The power performance and accumulated fatigue damage are presented in Fig. 5.8. The accumulated fatigue damage on the mooring lines of the wave parks decreases or remains relatively unchanged as the distance between the units increases. However, power performance does not show a consistent upward trend with increasing distance. Specifically, power performance decreases as the distance increases from 80 m to 100 m, but returns to its previous level as the distance further increases to 120 m. Additionally, the WaveEL 4.0 wave park outperformed its counterpart at 100 m and 120 m distances, demonstrating higher power performance and reduced accumulated fatigue damage. The results indicate that the interaction effects influence not only the power performance of the WECs but also the mooring fatigue damage.

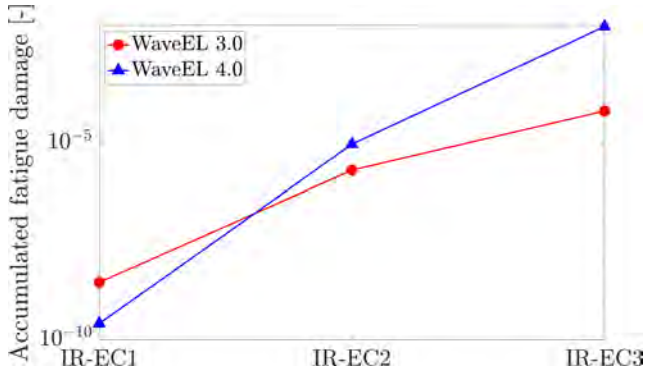

Figure 5.7: Accumulated fatigue damage of the weakest link of all mooring lines of Hex1-80 wave parks with different WEC versions and environment conditions.

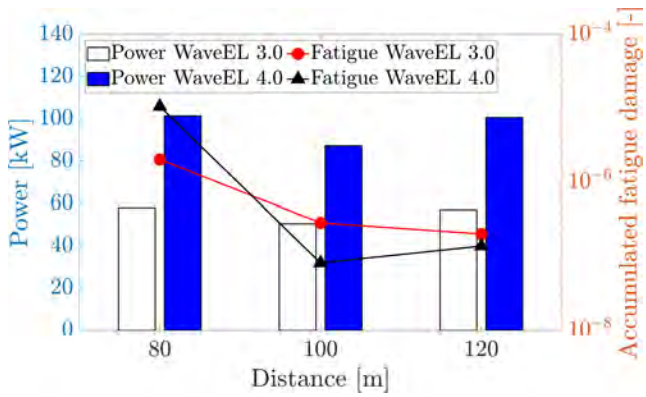

Figure 5.8: The accumulated fatigue damage and hydrodynamic power performance of wave parks with varying distances between the WECs under IR-EC2.

5.3 Summary of Paper C

"Hydrodynamic interactions and enhanced energy harnessing amongst many WEC units in large-size wave parks"

The DNV SESAM framework was applied to CorPower WEC, a bottom-fixed concept without mooring lines, in **Paper C**. Moreover, two layouts of a 16-WEC wave park equipped with CorPower were simulated. Parameters like the sea state, water depth, and wave direction were varied, and the results were compared to understand the features of CorPower wave parks.

The 4×4 wave park results under regular waves with varying wave periods and wave heights are compared in Fig. 5.9. It is observed from Fig. 5.9a that wave height significantly influences power performance, as power performances under conditions with a wave height of 4 m are generally higher than with a wave height of 1 m, for as the wave height increases fourfold from 1 m to 4 m, the power output experiences an increase of over tenfold. There is a range of wave periods from 7 s to 10 s where the power performances of the cases with a higher wave height suffer a significant drop.

Fig. 5.9b illustrates the interaction factors, defined as the ratio of power changes due to interaction effects to the power performance when these effects are disregarded. A positive interaction factor thus indicates constructive interaction effects. Although Fig. 5.9a shows that the performance drop for wave period from 7 s to 10 s is not significant for cases with lower wave heights, Fig. 5.9b reveals that the interaction factors in these cases are negative. This means that the interaction effects generally have destructive influences on power performances for both wave heights, with wave periods from 7 s to 10 s.

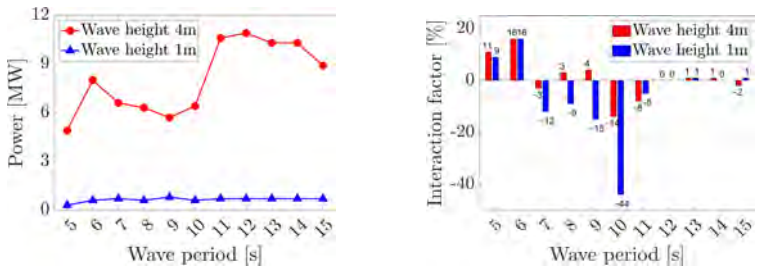

(a) Power performance. **(b)** Interaction factor.

Figure 5.9: The power performance and interaction factors of a 4×4 ($d = 150$ m) wave park under varying regular wave conditions.

The distance d between the WEC units in a 4×4 wave park was varied to study its effects on power performance. Fig. 5.10 shows the results for three cases with WEC distances of 50 m, 150 m, and 200 m, along with a reference case where interaction effects are ignored. For the terminology of the simulated cases, one can refer to Table

3 in **Paper C**. It can be observed that the WEC distance $d = 150$ m is optimal, as it results in a relatively large power performance increase under RL1 and RL2 while also avoiding a significant reduction in power output under RL3 to RL11.

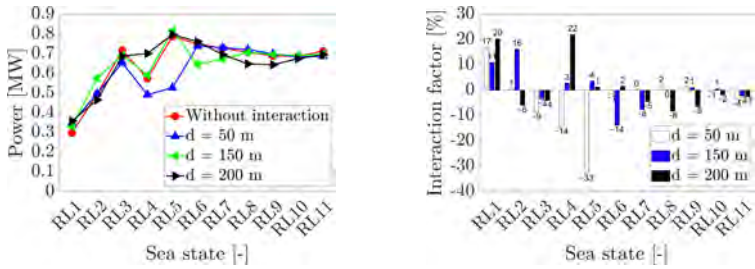

(a) Power performance. **(b)** Interaction factor.

Figure 5.10: The power performance and interaction factors of 4×4 wave parks with varying distances.

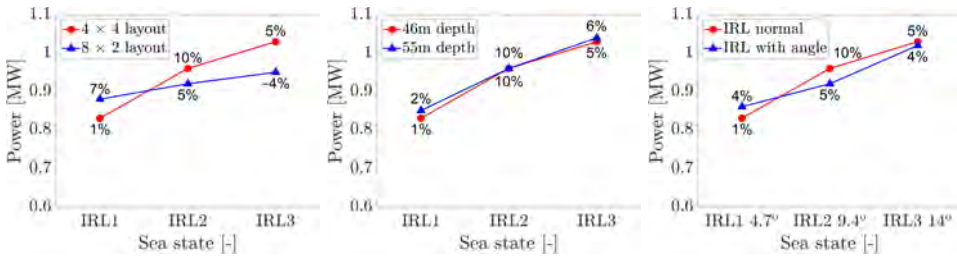

(a) **(b)** **(c)**

Figure 5.11: The total power performance of wave parks with (a) varying layouts, (b) varying water depths, and (c) wave directions of 4×4 wave park with d = 150 m. The percentages are the interaction factors, indicating the additional power generation due to interaction effects.

In addition to the regular wave cases, a few irregular wave cases were also simulated in **Paper C** to compare the power performance of cases with varying layouts, water depths, and wave directions. Fig. 5.11a presents the total power performance of the wave parks under three irregular wave cases. Most interaction factors are positive, except for the 8×2 wave parks under IRL3.

Two water depths were simulated, and the total power performances are shown in Fig. 5.11b. The interaction factors are positive for all three simulated irregular waves. The power performance of the 4×4 wave park with a WEC separation distance of 150 m does not differ significantly by water depth.

The wave direction for each irregular wave was determined based on the ECs at the anticipated installation site. As shown in Fig. 5.11c, the changed wave directions

result in minor drops in power performance under IRL2 and IRL3, but the interaction factors remain positive.

5.4 Summary of Paper D

"An FMI-based co-simulation framework for simulations of wave energy converter systems"

The aim of **Paper D** is to propose the FMI-based co-simulation framework. Two study cases demonstrate the features and capability of the FMI-based co-simulation framework: the first involving the single NoviOcean WEC described in Section 3.3, and the second examining the wave park described in Section 3.4.3, consisting of 18 NoviOcean WECs.

The numerical model for a single NoviOcean WEC was tested for regular waves with a wave amplitude of 1 m and a varying wave period from 3 s to 11 s. The relative motion between the buoy and the piston, shown in Fig. 5.12, depends on the wave period. For short-period waves (3–7 s), the relative motion amplitude is smaller than the wave amplitude (1 m), but matches the wave amplitude for longer wave periods (8–11 s). The buoy cannot respond to rapid wave excitation for very short wave periods (3–4 s), resulting in small relative motion. For wave periods of 5–7 s, the reduced relative motion is due to large surge motions, which can reach up to 9 m under 5 s waves, as shown in Fig. 5.13. As the wave period increases, surge motion decreases, staying within ±2 m for 9–11 s waves. The prismatic joint couples surge and heave motions, meaning that large surge motions limit heave amplitude. This highlights the importance of using a co-simulation approach to model such joints accurately.

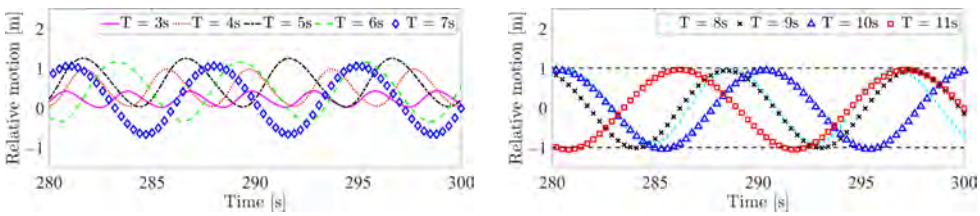

(a) Regular wave periods from 3 s to 7 s. **(b)** Regular wave periods from 8 s to 11 s.

Figure 5.12: Relative motions of the buoy and piston under regular waves with an amplitude of 1 m and varying wave periods. The dashed black lines indicate the range of wave elevation.

The damping coefficients of the linear damper PTO system model were set equal to the hydrodynamic radiation damping, as shown in Fig. 5.14. The time-averaged power performance of a single NoviOcean WEC, calculated using Eq. (2.13), is also

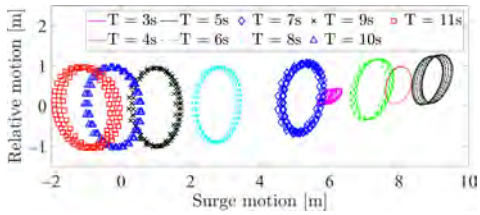

Figure 5.13: The surge motions versus the relative motion between the buoy and the piston.

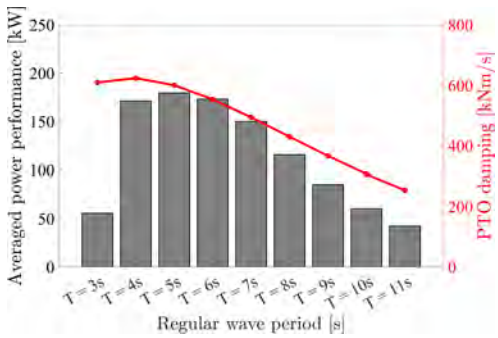

Figure 5.14: The averaged power performance of the WEC under regular waves with a constant wave amplitude of 1 m and varying wave periods.

presented for regular waves. While PTO damping peaks at a 4 s wave period, the highest power occurs at 5 s due to the effects of the mooring system's nonlinear stiffness on the WEC's dynamics. Therefore, time-domain simulations are essential for accurate power predictions when mooring systems are included.

Table 5.2: Parameters of the simulated irregular wave sea states for wave park simulations.

Sea states	H_s [m]	T_p [s]	Directions [deg]
1, 2, 3	0.9	9	0, 12, 24
4, 5, 6	1.8	9	0, 12, 24
7, 8, 9	2.7	9	0, 12, 24

Irregular wave sea states, based on the JONSWAP spectrum ($\gamma = 2.4$), were tested for the 18-WEC wave park of NoviOcean WEC to simulate real physical conditions. With a fixed peak period of 9 s, three significant wave heights (0.9, 1.8, and 2.7 m) and three wave directions (0, 12, and 24 degrees) were analysed for their effects on WEC dynamics and power performance. The wave parameters are summarised in Table 5.2.

Fig. 5.15 presents examples of the motion patterns of each WEC within the wave

park and displays the influence of the interaction effects. By comparing the vertical motion ranges of WECs in Figs. 5.15a to 5.15c, it is found that as wave height increases from 0.9 m to 2.7 m, heave motion amplitude rises. In comparison, surge motion range saturates when the wave height increases from 1.8 m to 2.7 m, peaking at −20 m to 5 m for the front-row WECs due to mooring system constraints. Wave direction mainly affects surge motion, with minimal impact on heave motion across the wave park. Moreover, it is also observed that the diffraction effect, a component of interaction effects, causes WECs at the rear of the wave park to experience smaller surge motions than those in the front. This demonstrates the co-simulation model's ability to capture interactions between multiple WECs. In Fig. 5.15d, as the wave direction changes from 0 to 12 to 24 degrees, the surge-sway trajectories tilt accordingly, with the sway motion range increasing as the wave direction shifts. This demonstrates that the co-simulation model accurately represents the features of the spherical joints.

The power performance of the 18-WEC wave park under various sea states is shown in Fig. 5.16a, which indicates that the WECs upstream tend to outperform those downstream. The upper range of the red, blue, and green background indicates the power performance of a single isolated WEC under the three sea states. Fig. 5.16b shows the total power performance of the entire wave park. The percentages indicate the power increase compared with an isolated single WEC. It is found that under all simulated sea states, the wave park generates more power than 18 isolated WECs, indicating that the interaction effects between the WECs are beneficial under the simulated conditions.

5.5 Summary of Paper E

"Integrating detailed power take-off system models in wave energy converter simulations using an FMI-based co-simulation approach"

Paper E emphasised the detailed PTO system modelling and its integration into the global model for single WECs and wave parks. The FMI-based co-simulation proposed in **Paper D** was adopted to integrate the detailed PTO system model described in Section 3.1.3 into the global WEC system model, including hydrodynamic, mechanical, and mooring systems. The study objects were a single WaveEL 3.0 WEC and a 6-WEC wave park, as in Fig. 3.10b. The simulated ECs included regular and irregular waves, as listed in Table 4.3 and 5.1.

Compared with the linear damper model, the detailed PTO system model incorporates the mechanisms of the PTO system components, as shown in Fig. 3.2, leading to distinct force and motion characteristics. Fig. 5.17 presents the time history of PTO force (F_{31}), the bumper force (F_{31b}), and the motion and velocity of the buoy hull (z_1, w_1) and water piston (z_3, w_3). Unlike the linear damper model, the PTO

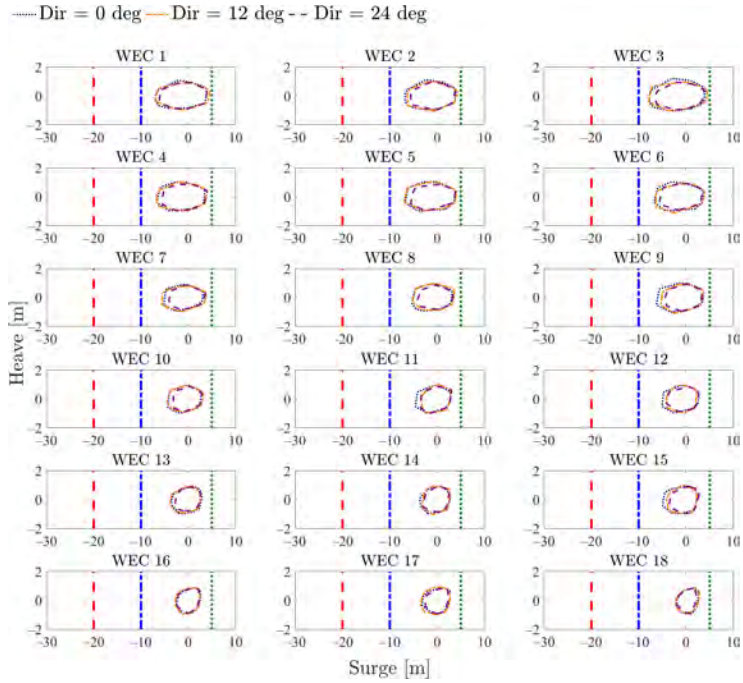

(a) Vertical motion under sea states 1, 2, 3.

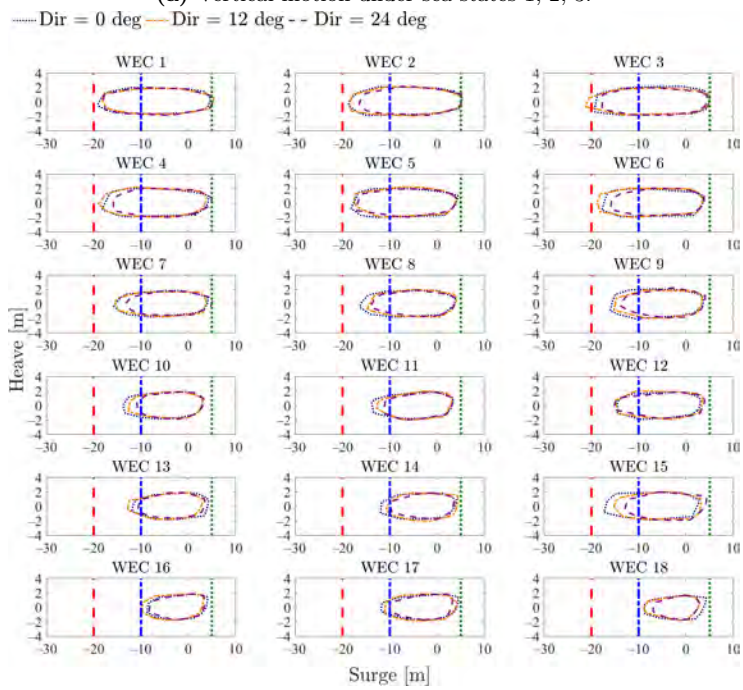

(b) Vertical motion under sea states 4, 5, 6.

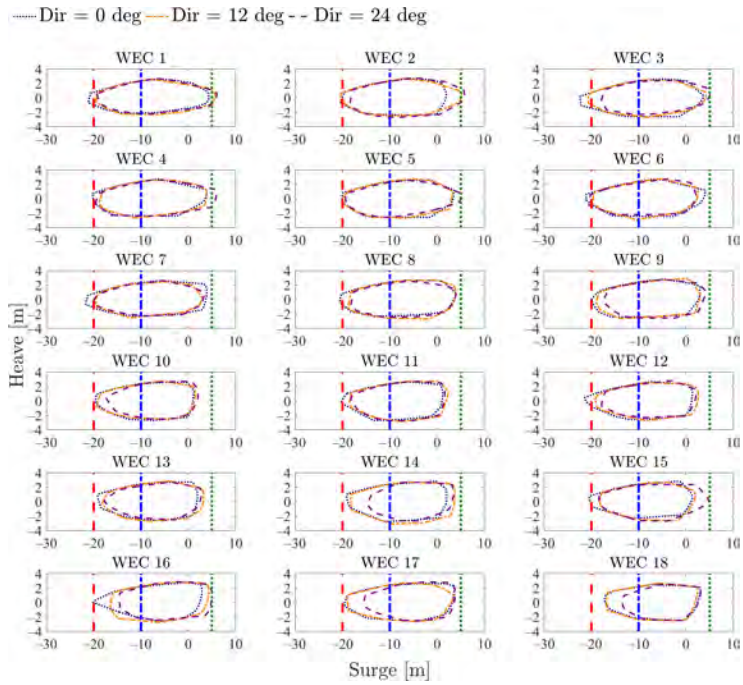

(c) Vertical motion under sea states 7, 8, 9.

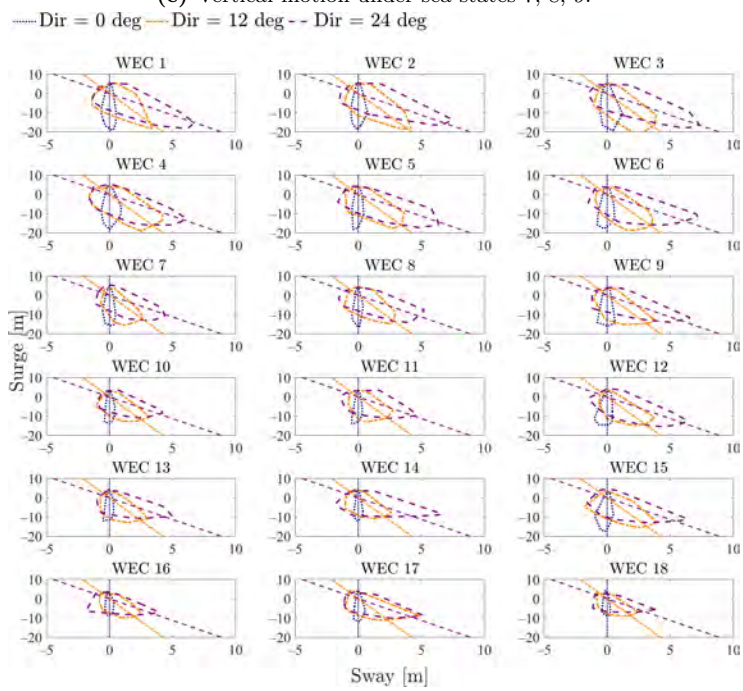

(d) Horizontal motion under sea states 4, 5, 6.

Figure 5.15: Example WEC trajectory under various sea states.

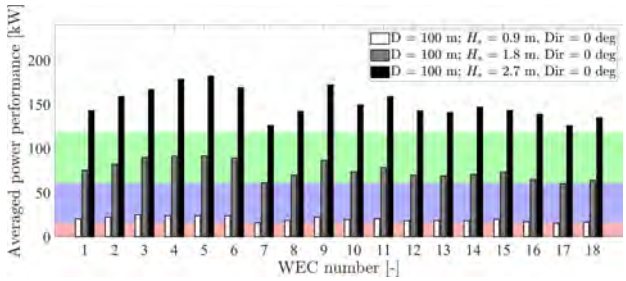

(a) Power performance of each WEC.

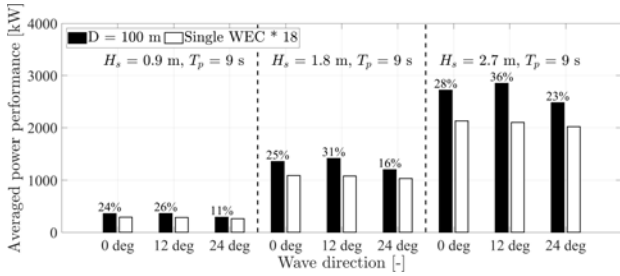

(b) Total power performance.

Figure 5.16: The power performance of each WEC and the total power performance of the wave park.

force (F_{31}) in the detailed PTO system model exhibits nonlinearity due to the hydraulic cylinder mechanism. The plateaus in the PTO force curves result from the dynamic valve opening conditions of the suction, outlet, and internal piston valves.

The bumper is designed to absorb substantial impacts from the water piston and restrict its motion. As shown in Fig. 5.17, it operates only under EC3 conditions. When the relative motion ($z_3 - z_1$) exceeds the 1.75 m stroke limit, the bumper applies a reactive force opposing the piston's motion. The peak bumper force, up to three times greater than the PTO force, significantly affects WEC motions.

The bumpers' restriction of the water piston reduces power performance under EC3 and IR-EC3, as shown in Fig. 5.18. While there are discrepancies between the linear damper model and the detailed PTO system model under lower wave heights, they can be mitigated by calibrating the damping coefficients of the linear damper model. However, when the bumpers are engaged, a detailed PTO system model becomes essential due to the significant impact of the bumpers on power performance.

Fig. 5.19 shows the interaction factors of the wave park under simulated wave conditions. The distance from each dot to the origin stands for the interaction factor, while the grey hexagon represents the unit interaction factor, here defined as the ratio of the power performance of each WEC within the park to that of a single WEC under the same conditions. Irregular waves tend to equalise the power performance

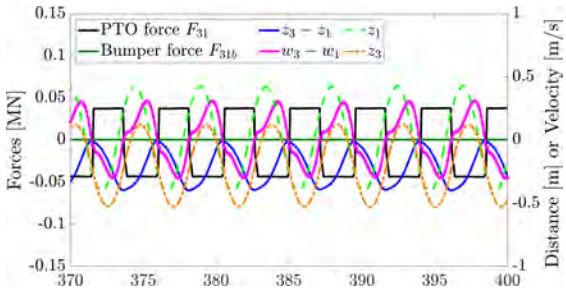

(a) EC1.

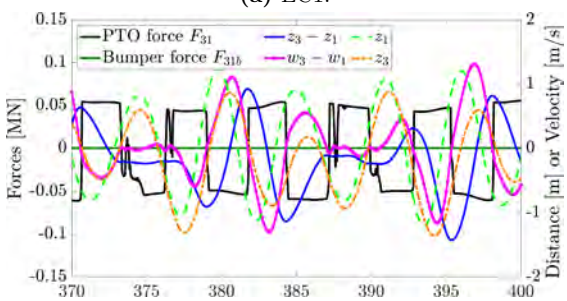

(b) EC2.

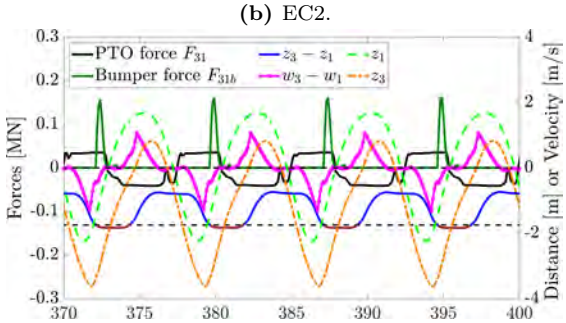

(c) EC3.

Figure 5.17: Forces and motions of a Single WaveEL 4.0 WEC under regular waves.

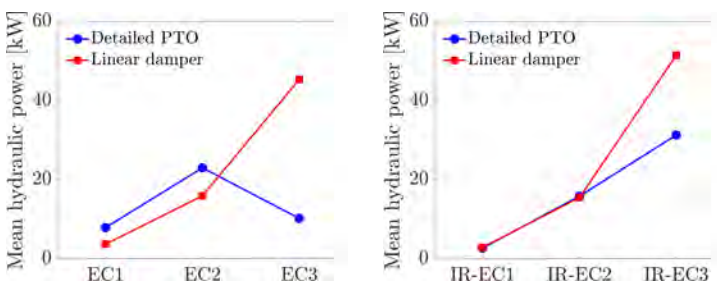

(a) Regular waves. **(b)** Irregular waves.

Figure 5.18: Single WEC power performance under regular and irregular waves.

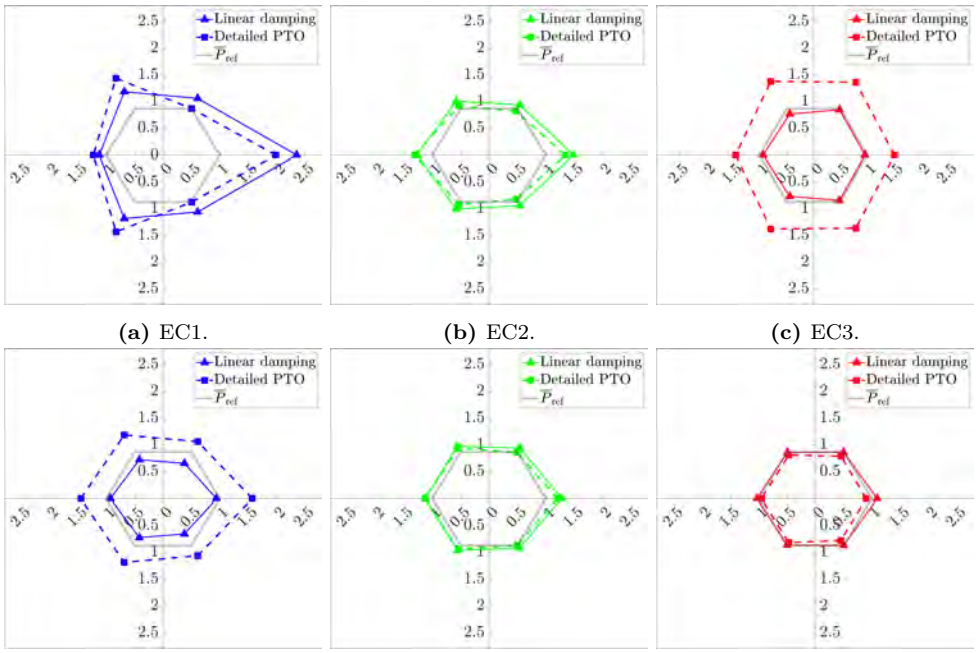

(a) EC1. **(b)** EC2. **(c)** EC3.

(d) IR-EC1. **(e)** IR-EC2. **(f)** IR-EC3.

Figure 5.19: Interaction factors under simulated wave conditions.

of each WEC due to wave component randomness. Under EC3, a notable difference arises: the interaction factors are equally distributed among WECs in both models, but the detailed PTO model yields a higher interaction factor (around 1.5) than the linear damper model (around 1). This is because, under EC3 the water piston hits the bumper, reducing power performance. However, in the wave park, the combined effects of radiation and diffraction lead to fewer bumper impacts, enhancing WEC performance over that of a single isolated WEC. Under IR-EC1, the interaction factors diverge significantly between the two models. The linear damper model predicts destructive interactions (factors < 1), while the detailed PTO model predicts positive interactions. This discrepancy suggests that the fidelity of the PTO system model heavily influences interaction factor predictions.

Besides power performance prediction, the fidelity of the PTO system model also affects the mooring fatigue damage predictions. Fig. 5.20 shows the largest mooring fatigue damage at the fairlead of each WEC unit, comparing simulations made with the linear damper and detailed PTO system models. The percentages indicate the relative increase in fatigue damage when switching from the linear damper to the detailed PTO model. Overall, the fidelity of the PTO system model plays a significant role in predicting mooring fatigue damage. The most notable difference is in M33

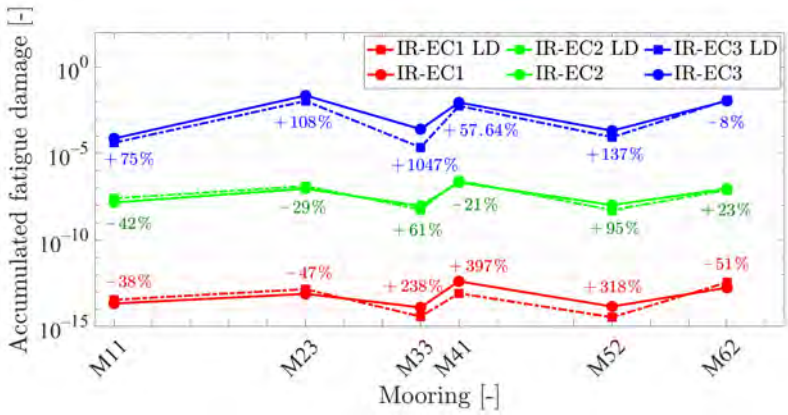

Figure 5.20: Comparison of the largest mooring fatigue damage of each WEC unit within the wave park at the fairlead under irregular waves using a linear damper PTO model and a detailed PTO model.

under IR-EC3, where the fatigue damage is approximately 10 times smaller than under the detailed PTO model. This underscores the importance of subsystem model fidelity, as it can significantly affect the results for other subsystems in the highly coupled global model.

CHAPTER 6

Discussion

This chapter provides a discussion mainly based on the results summarised in Chapter 5, as well as of a few other thoughts related to the overall content of the thesis. To better illustrate how each paper contributes to the research goals outlined in Section 1.2, Fig. 6.1 presents a diagram mapping the relationship between the papers and the defined goals.

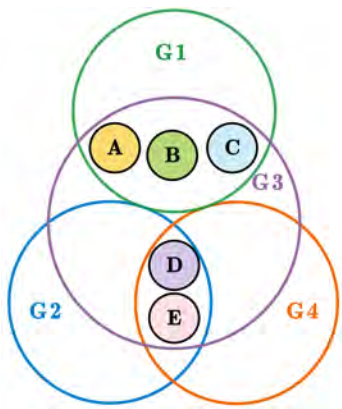

Figure 6.1: Goals and papers. **G1–4** are defined in Section 1.2.

Numerical modelling of WECs and limitations of the DNV SESAM framework

Papers A–C contribute to **G1** by developing numerical models for different WEC prototypes, both as single units and within wave parks, using the DNV SESAM framework.

While this framework successfully models WEC power performance in **Paper A** and mooring fatigue damage in **Paper B**, its limitations become evident in **Paper C** when applied to the bottom-fixed CorPower WEC concept without synthetic mooring lines. The reason is that the WEC studied in **Papers A** and **B** is a free-floating WaveEL WEC without explicit mechanical connections to the seabed, such as the rod of CorPower. Additionally, the PTO system of the WaveEL WEC was considered simple and was initially modelled as a linear damper, an assumption that was later partially disproven in **Paper E** under ECs when the nonlinear mechanism becomes significant. When the work in **Papers A–B** was carried out, the DNV SESAM framework was considered sufficient, which is why it was applied to model single WECs and wave parks in the early publications included in this thesis.

The unique working principles and components of CorPower, for example, the WaveSpring, pretension cylinder, and rod connected to the seabed, were modelled using necessary simplifications under the DNV SESAM framework in **Paper C**. However, it was realised that those simplifications were compromises necessitated by the limited capability of the DNV SESAM framework, which ultimately motivated the transition to the FMI-based co-simulation approach, which offers greater flexibility in integrating complex PTO and mechanical system models.

Development of an FMI-based co-simulation framework

Papers D–E contribute to **G2** by proposing, demonstrating, and developing an FMI-based co-simulation framework.

Paper D addresses the challenges of modelling and integrating complex WEC subsystems for global simulations by proposing an FMI-based co-simulation framework, allowing for the coupling of specialised numerical solvers with minimal programming effort. Using Ansys Aqwa and Rigid Dynamics for hydrodynamic loads and motion responses and Simulink for the PTO system, the framework integrates these subsystem models into a comprehensive global simulation for a single WEC unit or a wave park. This approach simplifies subsystem coupling and enhances system-level modelling efficiency.

In **Paper D**, the NoviOcean WEC was selected as the WEC prototype to be studied due to its complex subsystems. While the FMI-based co-simulation framework allows a detailed PTO system model to be coupled to the global simulation, the PTO system of the NoviOcean WEC was simplified as a linear damper due to the lim-

ited information available during the project. Nevertheless, this simplification does not undermine the capability of the proposed FMI-based co-simulation framework. In **Paper E**, for the WaveEL WEC, whose PTO system is better characterised, a detailed PTO system model was successfully developed and integrated into the global simulation within the FMI-based co-simulation framework, further demonstrating its potential.

Interaction effects in wave parks

All the papers contribute to **G3**, which is to investigate the interaction effects in wave parks equipped with various WEC concepts. The results indicate that multiple factors, including wave amplitude, wave period, wave direction, and WEC type, influence wave park power performance.

The 6-WEC WaveEL wave parks studied in **Paper A** and 18-WEC NoviOcean wave parks studied in **Paper D** exhibited enhanced power performance compared to isolated WECs under the simulated ECs. A common observation is that upstream WECs tend to outperform downstream WECs due to interaction effects. However, power performance predictions remain highly case-dependent, and no universal design rules can be established for optimal wave park configurations. Furthermore, **Paper E** highlighted that the level of modelling fidelity could also significantly impact the prediction of interaction effects on both power performance and mooring fatigue damage. Therefore, it is suggested that simulations of wave park designs should be carried out case-specifically, and the PTO system should also be modelled in enough detail to yield predictions close to reality.

The impact of PTO system model fidelity on global simulations

Papers D–E contribute to **G4**. **Paper E** is a milestone as it integrates detailed PTO system models into a wave park, which, to the best of the author's knowledge, other researchers have not done. It highlights the significant impact of the fidelity of the PTO system model on predictions of WEC motion, power performance, and mooring fatigue damage. This work paves the way for further research on the application of the FMI-based co-simulation framework to modelling WEC systems, which will better guide WEC design and the large-scale commercialisation of wave parks.

Technological niche

In this thesis, multiple wave parks have been simulated using the two proposed numerical frameworks. These simulations fill the niche of cases where the wave park

layouts and the number of units in a wave park are partly settled, and detailed analyses of power performance and mooring fatigue damage are needed for design iterations and decision-making before the installation. The FMI-based co-simulation framework allows each WEC model within a wave park to integrate detailed PTO, mechanical, and mooring systems, which highly increases the fidelity level of wave park simulations. The final goal of the wave park simulations in this thesis is not to find a theoretically optimal wave park layout but to analyse a few candidate layouts and provide accurate and detailed evaluations to support engineering design and development.

Verification and validation challenges

This numerical model of each WEC prototype could have received a more thorough validation if additional experimental data had been available. As more experimental data become available in the future, the numerical model can be calibrated by adjusting parameters such as the stiffness of the WaveSpring of CorPower in **Paper C** and the value of the damping coefficient of the PTO system model of WaveEL in **Paper E**.

At the time this thesis was written, experimental data for full-scale NoviOcean WECs were unavailable. Consequently, **Paper D** primarily focused on demonstrating the capability of the FMI-based co-simulation framework to simulate WECs consisting of multiple bodies, both as single units and in wave parks comprising up to 18 WECs. In the future, if experimental studies are available, the co-simulation numerical model can be fine-tuned and calibrated to better capture the actual behaviours of these systems. Moreover, the PTO system model used in **Paper D** is a simplified linear damper model since the PTO system details were unavailable during the study. This limitation can be mitigated if a detailed PTO system model is developed and exported as an FMU module, which can be easily integrated under the FMI-based co-simulation framework. This idea has been validated in the **Paper E** for the WaveEL 4.0 WEC.

Sensitivity analysis

Extensive simulations were conducted for multiple WEC prototypes and wave park configurations to examine the effects of varying wave height, wave period, wave direction, PTO damping coefficients, WEC versions, and wave park layouts. These parametric studies offer insights into how different environmental and design parameters influence WEC performance and hydrodynamic interactions. While not a formal sensitivity analysis from a statistical point of view, these simulations contribute to our understanding of the responses of the numerical frameworks to varying condi-

tions. The results are reasonable and can be explained, which justifies the capability of the numerical frameworks.

CHAPTER 7

Conclusions

This thesis proposed two numerical frameworks, DNV SESAM and FMI-based co-simulation frameworks, to handle the modelling of WECs and enable simulations at different fidelity levels. By applying these frameworks, three WEC prototypes with distinct working principles and designs were analysed regarding their power performance and mooring fatigue damage. The findings give us a deeper understanding of WEC behaviour under different modelling approaches. The key conclusions are summarised based on the research objectives outlined in Section 1.2.

Numerical models for single WECs and wave parks under the DNV SESAM framework

The DNV SESAM framework was applied to model single WECs and wave parks of WaveEL and CorPower WEC prototypes in **Papers A–C** under various wave conditions. The numerical model of WaveEL was validated by comparing the WEC motion with experimental data, demonstrating the capability of the DNV SESAM framework to simulate floating point absorbers with simple mechanical and PTO systems.

FMI-based co-simulation framework

The FMI-based co-simulation framework was proposed in **Paper D** to enable the detailed modelling of the mechanical and PTO systems of WECs by coupling solvers and tools without programming effort. Its capability to integrate subsystem models into a global model has been validated and verified by comparing the numerical

results from an experimental benchmark study of a dropping sphere and a numerical model of WaveEL developed under the DNV SESAM framework.

The NoviOcean WEC, which features a spherical ball joint connecting the piston rod to the seabed and a prismatic joint connecting the piston rod to the water tube, was chosen as a case study. It was modelled using the FMI-based co-simulation framework in **Paper D**. It was found that the prismatic joint couples surge and heave motions, leading to reduced heave motion when the surge motion is significant. Additionally, the spherical joint allows the buoy to rotate when the wave direction changes, causing it to tilt perpendicular to the wave direction. This example indicates that the mechanical system, such as the joint connections, needs to be modelled to capture the physical characteristics of WECs, which consequently leads to more accurate power performance and mooring fatigue damage predictions.

The results demonstrate that the FMI-based co-simulation framework provides a versatile and practical approach to model WECs with complex mechanical and PTO systems. Given its ability to integrate detailed subsystem models, this framework can be extended to other WEC prototypes with similar mechanical complexities, supporting more accurate performance predictions and design optimisation.

Influence of interaction effects on wave park power performance and mooring fatigue damage

6- and 10-WEC wave parks of WaveEL WECs and 16-WEC wave parks of CorPower WECs were simulated and analysed in **Papers A** to **C** using the DNV SESAM framework and simplified PTO system models. It was found that the power performance of a wave park is influenced by a variety of factors, including wave amplitude, period, direction, and different WEC designs, and should be analysed on a case-specific basis.

For the Hex1-80 wave park, under various wave directions, the leading mooring line consistently experiences the most significant accumulated fatigue damage. By adjusting the WEC distance of a wave park, it was found that there may be an optimal design point where the mooring fatigue damage and the total power performance can be balanced. This suggests that the mooring fatigue damage should be considered alongside power performance when evaluating the overall effectiveness of a wave park design.

An 18-WEC wave park of NoviOcean WEC was modelled and simulated using the FMI-based co-simulation to include its mechanical joints. It was found that the upstream WECs tend to outperform the downstream ones, and the total power performance of the entire wave park can be increased up to 36%.

The inclusion of a detailed PTO system model is crucial for accurately predicting power performance and mooring fatigue damage under ECs when nonlinear components, such as bumpers, come into play. The distribution of interaction factors in a 6-WEC wave park obtained from numerical models with a linear damper and a detailed PTO system was found to be similar under regular waves when the bumpers

are not engaged. However, under EC3 and simulated irregular waves (IR-EC1), the discrepancies in power performance between the two PTO system models become significant. The fidelity level of the PTO system model may heavily influence the prediction of mooring fatigue damage. In the simulated cases, it was found that the fatigue damage predicted by the linear damper PTO system model can be up to ten times smaller than that predicted by the detailed PTO system model. These findings highlight the importance of incorporating a detailed PTO system model to accurately predict interaction factors and mooring fatigue damage.

Integrating detailed PTO system into WEC system simulations

Benefiting from the proposed FMI-based co-simulation framework in **Paper D**, the detailed PTO system model was integrated into the WaveEL numerical model to form a global simulation in **Paper E**. It was found that the detailed PTO system model can capture the nonlinear features of the PTO due to dynamic valve opening conditions and reaction force from the bumper. Single WEC cases with a linear damper PTO system model and a detailed PTO system model were compared. It was found that the discrepancies in the power performance predictions of the two models hold under all simulated ECs. However, for ECs with lower wave heights, the discrepancies can be mitigated by calibrating the damping coefficients of the linear damper PTO model, while for ECs when the bumpers are engaged, the power performance predictions from the detailed PTO system model drop dramatically from those made by the linear damper model. This indicates that a detailed PTO system model is essential to reliably predict the power performance when nonlinear impacts are significant.

CHAPTER 8

Future work

Even though this thesis has achieved the goal of developing systematic numerical approaches for single WECs and wave park simulations, some aspects of the problem listed below can be studied in the future based on the foundation and knowledge provided by this thesis.

Integration with control strategies

Control algorithms can be applied to PTO systems to enhance power performance. For example, the parameters of the PTO system can be adjusted for different wave conditions to make the WECs move in better harmony with the waves to maximise the power performance. More advanced control algorithms can even orchestrate the parameters of each PTO system model of the WECs in a wave park separately to mitigate possible adverse interaction effects on power performance and improve the total power performance of the whole wave park. The FMI-based co-simulation framework provides convenience in coupling control algorithms to global numerical models to be tested and developed.

Hardware-in-the-loop development

From an industrial point of view, numerical simulations should be connected organically with experiments. There should not be a bias in over-reliance on either simulations or experiments. Instead, there needs to be a good balance in the development process. Integrating FMI-based co-simulation into Hardware-in-the-Loop (HIL) testing is a promising direction for future research. HIL testing requires high-

fidelity numerical models to interact with real hardware in real time, enabling the validation of control strategies and system behaviour before full-scale deployment.

FMI-based co-simulation provides a modular and scalable approach to HIL testing by allowing multi-domain models, such as hydrodynamic, mechanical, PTO, and control systems, to be coupled across different simulation environments. This enables the gradual integration of hardware components to reduce development risks and improve debugging efficiency.

Experiments for model calibrations and validations

Numerical analysis needs to be combined with experiments for WEC model calibrations and validations. In this thesis, limited experimental data were available to validate specific WEC models. Future work could include more WEC prototype experiments emphasising such aspects as hydrodynamic forces, PTO system performance, and mooring forces to calibrate and validate WEC numerical models from different perspectives.

Harsh ECs beyond the linear potential theory

Under harsh ECs, the WEC motions will be dramatic and the wave height will be large. The assumptions of the linear potential theory will then be violated. Therefore, to study the survivability of WECs under harsh environmental conditions, more advanced computational fluid dynamics (CFD) methods need to be applied to capture the hydrodynamic force accurately. In future works, to evaluate WEC performance under survival mode, a hydrodynamic model of WECs could be implemented in CFD software and integrated into the global model.

References

Ahamed, R., McKee, K., & Howard, I. (2020). Advancements of wave energy converters based on power take-off (PTO) systems: A review. *Ocean Engineering*, *204*, 107248.

Alves, M. (2016). Numerical modelling of wave energy converters. Elsevier.

Andersson, H., Holmberg, L. J., Simonsson, K., Hilding, D., Schill, M., Borrvall, T., Sigfridsson, E., & Leidermark, D. (2021). Simulation of leakage flow through dynamic sealing gaps in hydraulic percussion units using a co-simulation approach. *Simulation Modelling Practice and Theory*, *111*, 102351.

Andersson, H., Nordin, P., Borrvall, T., Simonsson, K., Hilding, D., Schill, M., Krus, P., & Leidermark, D. (2016). A co-simulation method for system-level simulation of fluid–structure couplings in hydraulic percussion units. *Engineering with Computers*, *33*(2), 317–333.

Andersson, H., Simonsson, K., Hilding, D., Schill, M., Sigfridsson, E., & Leidermark, D. (2019). Validation of a co-simulation approach for hydraulic percussion units applied to a hydraulic hammer. *Advances in Engineering Software*, *131*, 102–115.

Ansys, Inc. (2025a). Ansys Aqwa [Accessed: 2025-03-18]. https://www.ansys.com/products/

Ansys, Inc. (2025b). Ansys twin builder [Accessed: 2025-03-18]. https://www.ansys.com/products/digital-twin/ansys-twin-builder

Babarit, A. (2013). On the park effect in arrays of oscillating wave energy converters. *Renewable Energy*, *58*, 68–78.

Bao, X., Li, F., Sun, H., Iglesias, G., & Shi, H. (2023). Performance characteristics and parameter analysis of a multi-DOF wave energy converter with hybrid power take-off systems. *Energy Conversion and Management*, *278*, 116751.

Borgarino, B., Babarit, A., & Ferrant, P. (2012). Impact of wave interactions effects on energy absorption in large arrays of wave energy converters. *Ocean Engineering*, *41*, 79–88.

Bulian, G., & Cercos-Pita, J. L. (2018). Co-simulation of ship motions and sloshing in tanks. *Ocean Engineering*, *152*, 353–376.

Chang, G., Jones, C. A., Roberts, J. D., & Neary, V. S. (2018). A comprehensive evaluation of factors affecting the levelized cost of wave energy conversion projects. *Renewable Energy*, *127*, 344–354.

Chen, W., Wu, Z., Liu, J., Jin, Z., Zhang, X., & Gao, F. (2021). Efficiency analysis of a 3-DOF wave energy converter (SJTU-WEC) based on modeling, simulation and experiment. *Energy*, *220*, 119718.

Clément, A., McCullen, P., Falcão, A., Fiorentino, A., Gardner, F., Hammarlund, K., Lemonis, G., Lewis, T., Nielsen, K., & Petroncini, S. (2002). Wave energy in europe: Current status and perspectives. *Renewable and sustainable energy reviews*, *6*(5), 405–431.

CorPower Ocean. (2025a). CorPack - CorPower Ocean [Accessed: 2025-03-18]. https://corpowerocean.com/corpack/

CorPower Ocean. (2025b). Projects - CorPower Ocean [Accessed: 2025-03-18]. https://corpowerocean.com/projects/

CorPower Ocean. (2025c). Wave Energy Technology - CorPower Ocean [Accessed: 2025-03-18]. https://corpowerocean.com/wave-energy-technology/

Cummins, W., et al. (1962). The impulse response function and ship motions. *Technical Report 1661*.

Dang, H., Zhang, X., Li, B., Wen, J., & Sun, P. (2020). Multi-disciplinary co-simulation of floating process induced by pneumatic inflatable collar for underwater vehicle recovery. *Ocean Engineering*, *216*, 108008.

Dassault Systèmes. (2025). Dymola - system dynamics modeling [Accessed: 2025-03-18]. https://www.3ds.com/products/catia/dymola

De Castro, M., Lavidas, G., Arguilé-Pérez, B., Carracedo, P., De Castro, N., Costoya, X., & Gómez-Gesteira, M. (2024). Evaluating the economic viability of near-future wave energy development along the galician coast using lcoe analysis for multiple wave energy devices. *Journal of Cleaner Production*, *463*, 142740.

DNV. (2021). DNV-OS-E301: Offshore standards position mooring.

DNV. (2025a). Hydrodynamic analysis and stability analysis software - HydroD [Accessed: 2025-03-18]. https://www.dnv.com/services/hydrodynamic-analysis-and-stability-analysis-software-hydrod-14492/

DNV. (2025b). SESAM [Accessed: 2025-03-18]. https://www.dnv.com/services/strength-assessment-of-offshore-structures-sesam-software-1068/

Ecole Centrale de Nantes. (2025). NEMOH - A Boundary Element Methods (BEM) code for wave loads computation [Accessed: 2025-03-18]. https://lheea.ec-nantes.fr/research-impact/software-and-patents/nemoh-presentation

El Hammoumi, A., Chtita, S., Motahhir, S., & El Ghzizal, A. (2022). Solar pv energy: From material to use, and the most commonly used techniques to maximize

the power output of pv systems: A focus on solar trackers and floating solar panels. *Energy Reports*, *8*, 11992–12010.

European Commission. (2025). Competitiveness [Accessed: 2025-03-18]. https://commission.europa.eu/priorities-2024-2029/competitiveness_en

Falcão, A. F. d. O. (2010). Wave energy utilization: A review of the technologies. *Renewable and Sustainable Energy Reviews*, *14*(3), 899–918.

Falnes, J. (2007). A review of wave-energy extraction. *Marine Structures*, *20*(4), 185–201.

Gan, J., Zhou, Z., Yu, A., Ellis, D., Attwood, R., & Chen, W. (2023). Co-simulation of multibody dynamics and discrete element method for hydraulic excavators. *Powder Technology*, *414*.

Gao, H., Xiao, J., & Liang, R. (2024). Capture mechanism of a multi-dimensional wave energy converter with a strong coupling parallel drive. *Applied Energy*, *361*.

GeniE. (2025). Home page of GeniE [Accessed: 2025-03-18]. https://www.dnv.com/services/conceptual-modelling-of-offshore-and-maritime-structures-genie-89128

Ghafari, H. R., Ghassemi, H., Abbasi, A., Vakilabadi, K. A., Yazdi, H., & He, G. (2022). Novel concept of hybrid wavestar- floating offshore wind turbine system with rectilinear arrays of wecs. *Ocean Engineering*, *262*.

Giassi, M., Castellucci, V., & Göteman, M. (2020). Economical layout optimization of wave energy parks clustered in electrical subsystems. *Applied Ocean Research*, *101*, 102274.

Gu, H., Stansby, P., Zhang, Z., Zhu, G., Lin, P., & Shi, H. (2023). Research and concept design of wave energy converter on ocean squid jigging ship. *Energy*, *285*.

Guo, B., Ringwood, J. V., & Malca, C. (2021). A review of wave energy technology from a research and commercial perspective. *IET Renewable Power Generation*, *15*(10), 1143–1154.

Han, Z., Cao, F., Tao, J., Zhang, C., & Shi, H. (2024). Study on the energy capture spectrum (ecs) of a multi-DOF buoy with MMR-PTO damping. *Ocean Engineering*, *294*.

Hatledal, L. I., Skulstad, R., Li, G., Styve, A., & Zhang, H. (2020). Co-simulation as a fundamental technology for twin ships. *Modeling, Identification and Control: A Norwegian Research Bulletin*, *41*(4), 297–311.

He, G., Liu, C., Zhang, W., Luan, Z., & Zhang, Z. (2023). Numerical study of the effect of central platform motion on the wave energy converter array. *Ocean Engineering*, *286*.

International Energy Agency. (2023). *World energy outlook 2023* (Report).

International Renewable Energy Agency. (2019). Climate change and renewable energy: National policies and the role of communities, cities and regions [Ac-

cessed: 2025-03-18]. https://www.irena.org/-/media/Files/IRENA/Agency/Publication/2019/Jun/IRENA_G20_climate_sustainability_2019.pdf

ITEA4. (2025). Modelisar [Accessed: 2025-03-18]. https://itea4.org/project/modelisar.html

Jiao, J., Chen, Z., Xu, W., Bu, S., & Zhang, P. (2024). Asymmetric water entry of a wedged grillage structure investigated by CFD-FEM co-simulation. *Ocean Engineering*, *302*, 117612.

Jin, S., & Greaves, D. (2021). Wave energy in the UK: Status review and future perspectives. *Renewable and Sustainable Energy Reviews*, *143*, 110932.

Kabir, E., Kumar, P., Kumar, S., Adelodun, A. A., & Kim, K.-H. (2018). Solar energy: Potential and future prospects. *Renewable and Sustainable Energy Reviews*, *82*, 894–900.

Kaldellis, J., & Apostolou, D. (2017). Life cycle energy and carbon footprint of offshore wind energy. comparison with onshore counterpart. *Renewable Energy*, *108*, 72–84.

Kramer, M. B., Andersen, J., Thomas, S., Bendixen, F. B., Bingham, H., Read, R., Holk, N., Ransley, E., Brown, S., Yu, Y.-H., Tran, T. T., Davidson, J., Horvath, C., Janson, C.-E., Nielsen, K., & Eskilsson, C. (2021). Highly accurate experimental heave decay tests with a floating sphere: A public benchmark dataset for model validation of fluid–structure interaction. *Energies*, *14*, 269.

Liu, Y., Zheng, S., Liang, H., & Cong, P.-w. (2022). Wave interaction and energy absorption from arrays of complex-shaped point absorbers. *Physics of Fluids*.

López, I., Andreu, J., Ceballos, S., de Alegría, I. M., & Kortabarria, I. (2013). Review of wave energy technologies and the necessary power-equipment. *Renewable and Sustainable Energy Reviews*, *27*, 413–434.

MathWorks. (2025). Simulink - simulation and model-based design [Accessed: 2025-03-18]. https://www.mathworks.com/products/simulink.html

Modelica Association. (2025). Functional Mock-up Interface (FMI) Standard [Accessed: 2025-03-18]. https://fmi-standard.org/

Newman, J. N. (2017). *Marine hydrodynamics*. The MIT Press.

Novige. (2023). Life project [Accessed: 2025-03-18]. https://noviocean.energy/life-project/

Orcina. (2025). Orcaflex [Accessed: 2025-03-18]. https://www.orcina.com/orcaflex/

Papillon, L., Costello, R., & Ringwood, J. V. (2020). Boundary element and integral methods in potential flow theory: A review with a focus on wave energy applications. *Journal of Ocean Engineering and Marine Energy*, *6*(3), 303–337.

Polinder, H., & Scuotto, M. (2005). Wave energy converters and their impact on power systems. *2005 International conference on future power systems*, 9 pp.–9.

Ringsberg, J. W., Jansson, H., Örgård, M., Yang, S.-H., & Johnson, E. (2020a). Design of mooring solutions and array systems for point absorbing wave energy devices—methodology and application. *Journal of Offshore Mechanics and Arctic Engineering*, *142*(3), 031101.

Ringsberg, J. W., Yang, S.-H., Lang, X., Johnson, E., & Kamf, J. (2020b). Mooring forces in a floating point-absorbing wec system – a comparison between full-scale measurements and numerical simulations. *Ships and Offshore Structures*, *15*(sup1), S70–S81.

Shao, X. (2023). *Analysis of power performance and mooring fatigue damage for wave energy parks* [Licentiate thesis]. Chalmers University of Technology [Accessed: 2025-03-18]. https://research.chalmers.se/en/publication/535719

Shao, X., Yao, H.-D., Ringsberg, J. W., Li, Z., & Johnson, E. (2024). Performance analysis of two generations of heaving point absorber wecs in farms of hexagon-shaped array layouts. *Ships and Offshore Structures*, 1–12.

Sheng, W. (2019). Wave energy conversion and hydrodynamics modelling technologies: A review. *Renewable and Sustainable Energy Reviews*, *109*, 482–498.

Shi, Q., Xu, D., & Zhang, H. (2021). Performance analysis of a raft-type wave energy converter with a torsion bi-stable mechanism. *Energy*, *227*, 120388.

Sima. (2025). Home page of Sima [Accessed: 2025-03-18]. https://www.dnv.com/services/marine-operations-and-mooring-analysis-software-sima-2324

Sricharan, V. V. S., & Chandrasekaran, S. (2021). Time-domain analysis of a bean-shaped multi-body floating wave energy converter with a hydraulic power take-off using WEC-Sim. *Energy*, *223*, 119985.

Teixeira-Duarte, F., Clemente, D., Giannini, G., Rosa-Santos, P., & Taveira-Pinto, F. (2022). Review on layout optimization strategies of offshore parks for wave energy converters. *Renewable and Sustainable Energy Reviews*, *163*, 112513.

Têtu, A., & Fernandez Chozas, J. (2021). A proposed guidance for the economic assessment of wave energy converters at early development stages. *Energies*, *14*, 4699.

United Nations. (2012). Perspectives on sustainable energy for the 21st century [Accessed: 2025-03-18]. https://sustainabledevelopment.un.org/content/documents/1131Energy_SD21.pdf

Venzke, M., Shudrenko, Y., Youssfi, A., Steffen, T., Turau, V., & Becker, C. (2023). Co-simulation of a cellular energy system. *Energies*, *16*, 6150.

WAMIT, Inc. (2025). WAMI [Accessed: 2025-03-18]. https://www.wamit.com/

Waves4Power. (2025a). The first tests of wave power at runde are now accomplished and the wave power buoy waveel 3.0 is towed to fiskaholmen [Accessed: 2025-03-18]. https://www.waves4power.com/the-first-tests-of-wave-power-at-runde-are-now-accomplished-and-the-wave-power-buoy-waveel-3-0-is-towed-to-fiskaholmen/

Waves4Power. (2025b). Five months and going strong [Accessed: 2025-03-18]. https://www.waves4power.com/five-months-and-going-strong/

Waves4Power. (2025c). Technology [Accessed: 2025-03-18]. https://www.waves4power.com/technology/

Wei, Z. W., Shi, H. D., Cao, F. F., Yu, M. Q., Li, M., Chen, Z., & Liu, P. (2024). Study on the power performance of wave energy converters mounted around an offshore wind turbine jacket platform. *Renewable Energy*, *221*, 119786.

World Wide Fund for Nature. (2023). Global energy policy framework [Accessed: 2025-03-18]. https://wwfint.awsassets.panda.org/downloads/wwf-global-energy-policy-framework_1.pdf

Yang, S.-H., Ringsberg, J. W., & Johnson, E. (2017a). Parametric study of the dynamic motions and mechanical characteristics of power cables for wave energy converters. *Journal of Marine Science and Technology*, *23*(1), 10–29.

Yang, S.-H., Ringsberg, J. W., & Johnson, E. (2020). Wave energy converters in array configurations—influence of interaction effects on the power performance and fatigue of mooring lines. *Ocean Engineering*, *211*, 107294.

Yang, S.-H., Ringsberg, J. W., Johnson, E., & Hu, Z. (2017b). Biofouling on mooring lines and power cables used in wave energy converter systems—analysis of fatigue life and energy performance. *Applied Ocean Research*, *65*, 166–177.

Yang, S.-H., Ringsberg, J. W., Johnson, E., Hu, Z., & Palm, J. (2016). A comparison of coupled and de-coupled simulation procedures for the fatigue analysis of wave energy converter mooring lines. *Ocean Engineering*, *117*, 332–345.

Yuan, R., Fletcher, T., Ahmedov, A., Kalantzis, N., Pezouvanis, A., Dutta, N., Watson, A., & Ebrahimi, K. (2020). Modelling and co-simulation of hybrid vehicles: A thermal management perspective. *Applied Thermal Engineering*, *180*, 115883.

Zhang, J., Zhao, X., Greaves, D., & Jin, S. (2023). Modeling of a hinged-raft wave energy converter via deep operator learning and wave tank experiments. *Applied Energy*, *341*, 121072.

Zou, S., Robertson, B., Roach, A., Mundon, T., Rosenberg, B., & Penalba, M. (2024). Wave energy converter arrays: A methodology to assess performance considering the disturbed wave field. *Renewable Energy*, *229*, 120719.